2016-06-01

Microfabrication with Smooth, Thin CNT/Polymer Composite Sheets

Nathan Edward Boyer
Brigham Young University - Provo

Microfabrication with Smooth, Thin CNT/Polymer Composite Sheets

Nathan Edward Boyer

A thesis submitted to the faculty of
Brigham Young University
in partial fulfillment of the requirements for the degree of

Master of Science

Robert Davis, Chair
Richard Vanfleet
David Allred

Department of Physics and Astronomy

Brigham Young University

June 2016

ABSTRACT

Microfabrication with Smooth, Thin CNT/Polymer Composite Sheets

Nathan Edward Boyer
Department of Physics and Astronomy, BYU
Master of Science

Carbon nanotube (CNT)/polymer composite sheets can be extremely high strength and lightweight, which makes them attractive for fabrication of mechanical structures. This thesis demonstrates a method whereby smooth, thin CNT/polymer composite sheets can be fabricated and patterned on the microscale using a process of photolithography and plasma etching. CNT/polymer composites were made from CNTs grown using chemical vapor deposition using supported catalyst growth and floating catalyst growth. The composite sheets had a roughness of approximately 30nm and were about 6μm or 26μm depending on whether they were made from supported catalyst grown or floating catalyst grown CNTs. The composites were patterned using an oxygen plasma as the etchant and a hard mask of silicon nitride.

ACKNOWLEDGMENTS

TABLE OF CONTENTS

LIST OF FIGURES

LIST OF TABLES

Chapter 1
Introduction

In the last twenty years a great deal of research has been done on carbon nanotubes

(CNTs). Probing the properties of CNTs has revealed that they have a tensile strength and a

Young's modulus of around 100 GPa[1], and 1 TPa[2], respectively, as well as electric and thermal

conductivities of approximately 1×10^8 S/m and 3000 W/mK, respectively[3,4]. For comparison,

A36 steel has an ultimate tensile strength of 0.55 GPa and Young's modulus of 207 GPa[5], and

copper has an electrical conductivity of 5.96×10^7 S/m and a thermal conductivity of 483 W/mK[6].

CNTs are 180 times stronger and almost 5 times stiffer than steel and have an electrical

conductivity comparable to copper while being 6 times more thermally conductive. To date

CNTs are one of the strongest, stiffest, most conductive materials known to man. This has led

researchers to explore applications of CNTs in electrical components, microelectromechanical

systems (MEMS), and composites.[7-29] Specifically, CNT composites have garnered much

attention because of the ability to give the properties of CNTs to the composite as a whole.[13-29,40,42,46-49]

Matrix materials for CNT composites have been both organic and inorganic. Examples

of matrix materials include silicon, metals, and polymers.[13,14,40,47-49] Hutchison et al. made

CNT/polysilicon composite microstructures by depositing silicon on and into a CNT forest.[13]

Barrett et al. made CNT/nickel composite structures by electroplating CNT forests with nickel.[14]

CNT/polymer composites have been used to make sensors and actuators.[8,22,36] Yun et al. made a

CNT/cellulose composite that was used to make an electro-active actuator.[42] CNT/polymer

composites have also been made stronger than the polymer alone.[20,28,29,46] For example, Spinks

et al. made a CNT/polyaniline composite which showed a 50 % increase in tensile strength when

compared to the polyaniline alone.[46]

1

This work will be focusing on creating CNT/polymer composites and patterning them with photolithography and plasma etching. Research presented in this thesis is split into two projects. The first project was making a CNT sheet that was about 6 μm thick with aligned CNTs, impregnating it with a polymer to make a composite and measuring the tensile strength and Young's modulus of the composite. The second project was taking a roughly 30 μm thick CNT sheet, impregnating it with polymer, and patterning it with photolithography and plasma etching to fabricate microstructures.

In the following background section, details are given about prior CNT/polymer composite research with a focus on that research which is supportive of both parts of this project. The introductions to the individual projects will discuss CNT/polymer composite research that applies to creating CNT/polyimide composites with aligned CNTs or to patterning CNT/polyimide composites, respectively. The rest of this introduction serves to familiarize the reader with various processes and machines that were used to make and process the CNT/polymer composites, as well as the tools and machines used to characterize the composites.

Background

CNT/polymer Composites

In studying strong CNT/polymer composites, researchers have reported a wide range of tensile strengths. Zhou et al. made CNT/epoxy composites with 3 wt% CNTs that have an average tensile strength of 121 MPa.[29] Zhou et al. reported epoxy without CNTs had a tensile strength of 93.5 MPa, which is a 28.3% increase of tensile strength in the composite. They started making their CNT/epoxy composites by sonicating CNTs in the first part of the epoxy, Epon 862. Following that, the second part of the epoxy, EpiCure curing agent W, was added and

mixed into the CNTs and Epon 862, then the entire mixture was poured into a mold and cured. Zhu et al. made a CNT/polyimide composite with functionalized CNTs which form bonds with the polyimide. They found that their composite had a tensile strength of 133 MPa.[28] CNTs were sonicated in a mixture of sulfuric acid and nitric acid which functionalized the CNTs by creating reactive oxidation sites on their surface. The CNTs were then separated from the acids and sonicated in N,N-dimethylacetamide (DMAc). The CNT/DMAc mixture was added to a solution of DMAc, 4,4'-oxydianiline, and pyromellitic dianhydride. This mixture was then poured into a mold and the DMAc evaporated, while the rest of the mixture was cured creating CNT/polyimide composites. These composites have much lower tensile strengths compared to individual CNTs. One of the barriers that prevents them from utilizing the whole strength of the CNTs is not being able to effectively bind the polymer to the CNTs.[16,17] In tensile testing, this leads to the CNTs being pulled out of the polymer instead of breaking.

Recently, several research groups have been able to make CNT/polymer composites that are more than 10 times stronger than the earlier composite examples by increasing the CNT density in the composites, increasing the length of the CNTs, functionalizing the CNTs, aligning the CNTs in the composite, and/or layering the CNTs and the polymer.[15-21] One should note that even though Zhu et al. functionalized their CNTs, they were also significantly shortened and weakened by sonication, which has been shown to damage CNTs.[28,30]

Cheng et al.[16] achieved much higher strengths in their CNT/bismaleimide composites by using aligned, millimeter-long CNTs that were functionalized and then using a hot press step to tightly pack the composite and remove voids. Their composites reached a strength of 3.1 GPa and a stiffness of 350 GPa. Cheng et al. started with sheets of CNTs grown by floating catalyst chemical vapor deposition (CVD) (produced by Nanocomp Inc.). They then stretched the CNT

sheets to align the CNTs. The CNTs were functionalized in a solution of m-CPBA and dichloromethane and subsequently washed with dichloromethane to remove residual m-CPBA. After the CNT sheets were dried, they were dipped in bismaleimide 5250-4 resin to impregnate the CNT sheets. CNT/bismaleimide composites were cured during hot pressing.

Wang et al.[17] made CNT/bismaleimide composites that achieved high strengths by using long CNTs in a process of aligning and layering CNTs with bismaleimide. Their CNT/bismaleimide composite reached a strength and stiffness of 3.8 GPa and 293 GPa, respectively. Wang et al. started with a CNT forest grown by supported catalyst CVD. The CNTs were drawn out across rods to align the CNTs, then they were wound around a spool while being sprayed with bismaleimide resin. The CNT/bismaleimide composites were removed from the spool and cured.

Another method similar to what Wang et al. used was developed by Liu et al.[18] Liu et al., in addition to aligning and layering long CNTs with bismaleimide, used a hot-pressing process to tightly pack the composite and achieved a tensile strength of 4.5 GPa and a Young's Modulus of 275 GPa. Liu et al. began with a CNT forest that they grew by supported catalyst CVD. The CNTs were drawn out of the forest and wound around a spool while being sprayed with bismaleimide resin. The CNT/bismaleimide composite was dried and stretched, and afterwards was hot pressed and cured.

While these research groups created CNT/polymer composites that are the strongest to date, these composites are still far weaker than individual CNTs, but CNT/polymer composites could potentially become as strong as individual CNTs by increasing the lengths and densities of the CNTs in the composites.[16,21] However, as micromechanical structures these composites are already very interesting because their strength is comparable to that of crystalline silicon,

4

currently the most widely used micromechanical material. The tensile strengths of crystalline silicon ranges from 1 GPa to 7 GPa.[31,32] These composites are also between 1.5 and 7 times stiffer than crystalline silicon which has Young's moduli between 50 GPa and 190 GPa.[33] Stiffness affects the resonance frequency of a material, and since these composites are 1.5 to 7 times stiffer than silicon and half as dense, they would have resonance frequencies between 1.7 to 3.7 times higher. The goal of this research is to determine if high CNT density composites can be effectively patterned using standard microfabrication techniques making them attractive for MEMS and other similar fields.

Microfabrication Processes

Thin film microfabrication processes used in this project include additive, subtractive, and patterning processes.[44] In additive processes, a thin film of material is deposited over the whole substrate. Examples of additive processes include chemical vapor deposition (CVD), which uses molecular gases to deposit materials (fig 1.1a), and physical vapor deposition (PVD), which includes sputtering and evaporating materials (fig 1.1b). In subtractive processes,
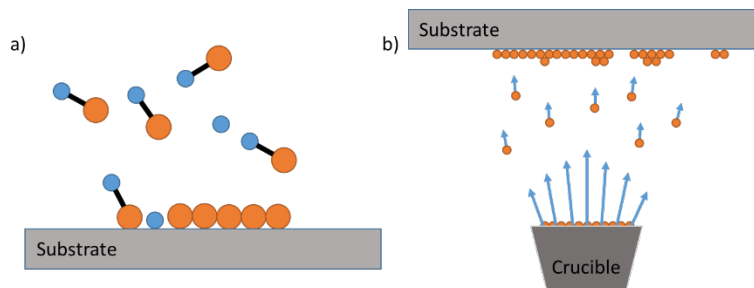
Figure 1.1 a) An illustration of gas molecules decomposing and depositing on a substrate in a CVD system. b) An illustration of atoms evaporating from a crucible and depositing on a substrate in an evaporator.
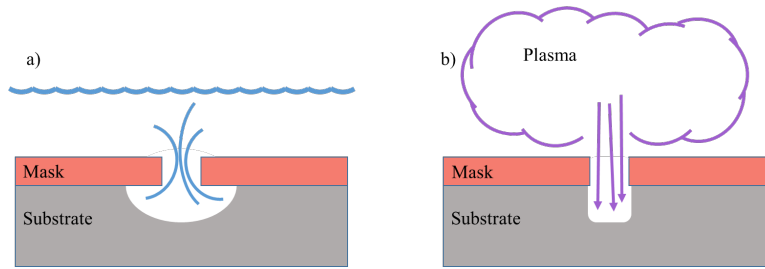
Figure 1.2 a) An illustration depicting how typical wet etching works. Chemicals in the liquid react with the substrate material, essentially dissolving the substrate. The substrate is etched at the same rate in all directions making a circular hole. b) An illustration depicting how typical dry etching works. Gases react with the substrate material creating volatile molecules that leave the substrate. In this example of dry etching the gases are ionized and directed at the substrate, creating a more vertical hole.

materials are etched or removed using a variety of chemicals and gases depending on the material to be etched. Examples of subtractive processes include wet etching, which uses a liquid solution to remove material (fig 1.2a), or dry etching, which uses gases and plasmas to remove material (fig 1.2b). In pattering processes, a light sensitive chemical called photoresist is deposited on the substrate and select areas of the photoresist are exposed to light; then developed using a chemical developer leaving patterned photoresist on the substrate. Then either an additive or subtractive process is used to deposit a patterned film or remove exposed material, respectively.

There are many variations of CVD systems, but the two that were used in these projects are: 1) a hot walled CVD system, and 2) a plasma enhanced CVD system (PECVD). In a hot walled CVD system, gases flow into the system and are heated. The heated gases then decompose and deposit on the substrate. The undecomposed gases and volatile products of the reaction are taken out of the system. The gas flows are controlled by mass-flow controllers (MFCs), which provide accurate control of how much of each gas is flowing in the CVD system and also allows for the gases to be shut off from the system when they are not needed. For many deposition materials, the gases need to be heated up to many hundreds of degrees Celsius or

6

higher. Silicon nitride, for example, is typically deposited at 900 °C from silane (SiH_4) and ammonia (NH_4).[45] In order to deposit materials at lower temperatures, the gas must be decomposed by another source of energy, such as a plasma.

PECVD systems use heat and plasma to decompose gases for deposition. Inside the chamber of a PECVD, a plasma is generated between two parallel plates, and the sample is placed on one of the plates that is heated. Outside of the chamber, a PECVD system is very similar to a CVD system, with MFCs controlling gas flow. However, a PECVD system also uses a vacuum pump to keep the chamber at a lower pressure during deposition. In a PECVD system, the plasma helps decompose the gas so deposition can take place at lower temperatures. For example, silicon nitride can be deposited between 250 °C and 300 °C in a PECVD system from silane and ammonia as opposed to the 900 °C in a CVD system.[45]

A third system to deposit materials that were used was an evaporator. An evaporator deposits materials by heating them until they evaporate and then allowing them to condense on the sample and everywhere else in the chamber. Two different kinds of evaporators were used in these projects: a thermal evaporator and an electron beam evaporator. For thermal evaporators, the material to be deposited is in an alumina (Al_2O_3) coated tungsten wire basket and is heated by resistive heating of the tungsten wire basket with a high voltage. For an electron beam evaporator, the material to be deposited is in a crucible and a beam of electrons is focused on the material causing it to heat up and evaporate. In both evaporators, a quartz crystal monitor is used to measure the thickness of the film being deposited.

Wet and dry etching allows researchers to remove silicon and other material in a more precise manner than with traditional machining. Both types of etching can use a mask to protect
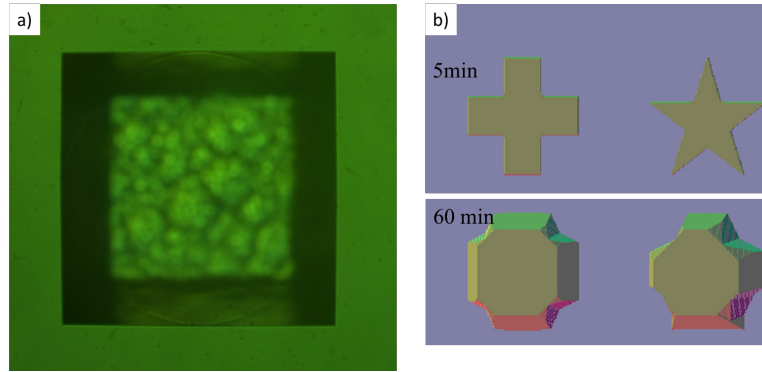
Figure 1.3 a) A hole produced by etching (100) silicon with KOH after 2 hr. The mask for the etch is still faintly visible on the top and bottom of the hole. Sample courtesy of the BYU Cleanroom. b) An Anisotropic Crystalline Etch Simulation (ACES) of KOH etching of silicon on the (100) plane after 5 min and 60 min. ACES was programed by the Micro Actuators, Sensors and Systems Group at University of Illinois at Urbana-Champaign.

parts of the sample while leaving other parts exposed to the etchant (fig 1.2). Ideally, the mask used in etching should be resistant to the etchant,[44] but at a minimum the mask should be able to survive the length of the etch.

Many wet etches are isotropic in nature, meaning they etch in all directions at the same rate, but there are several that are anisotropic. An example of an isotropic etch is using hydrofluoric acid (HF) to etch silicon dioxide. A common example of an anisotropic etch is using a solution of potassium hydroxide (KOH) and water to etch single crystal silicon. The KOH etches the silicon (111) crystal plane the slowest, which gives silicon the ability to have square etch patterns instead of rounded square etch patterns (fig 1.3).

Dry etches can also be isotropic, anisotropic, or anywhere in between depending on the etch conditions.   Using vapors or heated gases as an etchant will result in a more isotropic etch because the etchant does not have a preferred direction (unless crystal orientation plays a part). Plasmas can be anywhere between isotropic or anisotropic depending on how they are generated. Plasmas generated in inductively coupled plasma (ICP) systems are more isotropic in nature because the plasma generation does not give the ions a directional preference (fig 1.4). Plasmas

8
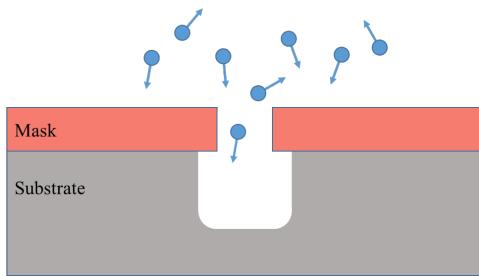
Figure 1.4 In non-directional dry etching the gases or gas ions move about randomly, which causes undercutting of the mask.
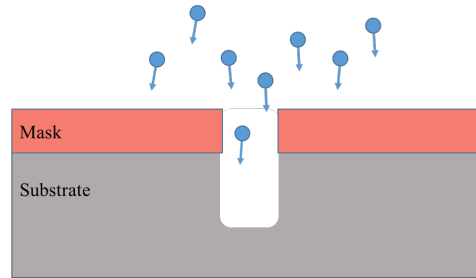
Figure 1.5 In directional dry etching the gases or gas ions impact the substrate vertically, which causes less undercutting of the mask and a more vertical etch.

Accelerating Voltage	Magnification	Spot Size	Working Distance	
10 kV	20000 x	3	13.1 mm	2 µm
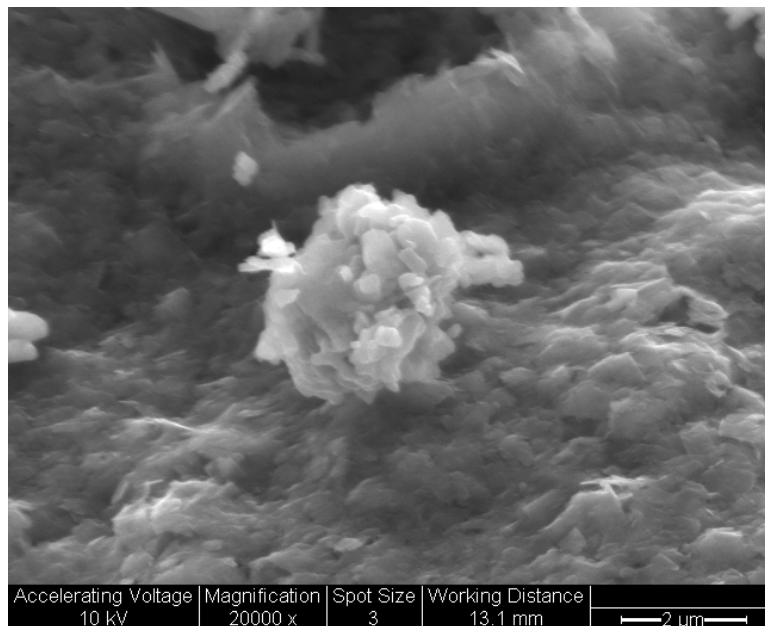
Figure 1.6 An example of an image taken with an SEM. The scale bar is 2µm.

generated in parallel plate systems, or reactive ion etchers (RIE), are more anisotropic because

the parallel plates cause the ions to move perpendicular between the plates (fig 1.5). In this

research, an oxygen plasma is used to dry etch CNTs. This etch is carried out in an ICP RIE

system, which controls the power to generate the plasma and the power to accelerate the ions

independently of each other. Separating the power for plasma generation and the power for ion

acceleration enables the generation of a dense plasma with a small directional component.

Scanning Electron Microscope

The scanning electron microscope (SEM) is an instrument used in examining samples on

a microscopic scale. Some of the information that can be gathered through an SEM includes

sub-micron resolution images, elemental composition, crystal structure, and crystal orientation.

An SEM works by generating a beam of electrons and focusing that beam on a sample. When

the electrons from the beam strike the sample they produce backscattered electrons, secondary

electrons, Auger electrons, and x-rays. Backscattered and secondary electrons are usually

detected with an Everhart-Thornley (ET) Detector which reads the electrons coming in as an

Lsec: 30.0 0 Cnts 0.000 keV Det: Octane Plus Det
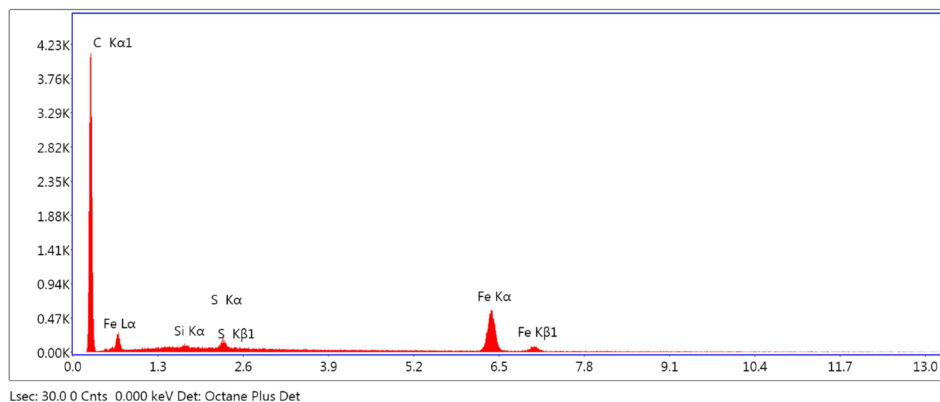
Figure 1.7 An x-ray spectrum collected in an SEM. The peaks on the plot
correspond to different electron energy transitions in each element present in
the sample. The horizontal axis is energy in keV and the vertical axis is
intensity.

10

electric current. To make an image, the SEM scans the beam of electrons in a raster on the

sample and at each point in the raster the electric current from the ET detector is measured. The

SEM then assigns an intensity between black and white at each point proportional to the current

measured and an image is made (fig 1.6). The x-rays that are generated at the sample are used to

detect the elemental composition of the sample being imaged by exciting electrons and holes in a

silicon crystal, which then produces an electrical current that is proportional to the energy of that

x-ray. Counting the number of x-rays at each energy level will produce a spectrum (fig 1.7) and

comparing peaks in that spectrum to characteristic x-rays from different elements reveals the

elemental composition.

Chapter 2
Carbon Nanotube Composite Sheets from Horizontally
Aligned Carbon Nanotubes

Introduction

In CNT/polymer composites, alignment of CNTs has been shown to be important to the strength of the composites. Cheng et al.,[16] Wang et al.,[17] and Liu et al.,[18] whose research was discussed in the background section, measured the differences in strength between stretched and unstretched composites. In the paper from Cheng et al., the strength of a CNT/bismaleimide composite that was unstretched and functionalized was 1.4 GPa, while the composite that was stretched and functionalized had a strength of 3.1 GPa. Stretching the composite gave it a strength that was double that of the unstretched composite. Wang et al. and Liu et al. saw the strength of their composites improve 1.9 times and 2 times, respectively, by stretching them to align the CNTs.

Wang et al.[35] and Bradford et al.[21] aligned CNTs in their CNT sheets (buckypaper), not by stretching the sheets but by knocking down vertically aligned CNTs in forests. Wang et al.[35] made a CNT sheet by placing a porous membrane on a grown CNT forest, and using a roller, they forced the CNTs down in the same direction. The CNT sheet was then peeled off the growth substrate with the porous membrane and released from the membrane by washing it with ethanol. Bradford et al.[21] made a CNT/epoxy composite by growing a CNT forest and applying a shear force at an angle to the top of that CNT forest, which pushed the forest over and down, making it a sheet. They were then able to peel the CNT sheet from the growth substrate and soak the CNT sheet in epoxy resin. The strength of the CNT sheet was 16 MPa, which Bradford et al. cited as being typical of buckypapers. The strength of the CNT/epoxy composite was 300 MPa.

Even though the CNT/epoxy composites made by Bradford et al. were not as strong as the CNT composites from Cheng et al.,[16] Wang et al.,[17] and Liu et al.,[18] they would still be useful in many applications because they are strong and thin. In this research, we demonstrate a method to fabricate CNT/polyimide composites by growing CNT forests by supported catalyst CVD growth, then knocking them over with a polytetrafluoroethylene (PTFE) cylinder, similar to how Wang et al.[35] knocked over their CNT forests. Impregnating the CNT sheet with polyimide, hot pressing and curing completes the final CNT/polyimide composite.

Process

Making our CNT/polyimide composite with knocked down CNTs consisted of two main parts. The first was making a CNT sheet by preparing the substrate, growing the CNTs by supported catalyst CVD growth on the substrate and knocking over the CNTs. The second part was making the final CNT/polyimide composite by impregnating a CNT sheet with polyimide (PI-2610 produced by HD MicroSystems), curing the polyimide, and releasing the composite from the substrate.

Patterned CNT Growth

The patterned bilayer catalyst for CNT growth consisted of 4 nm of patterned iron on 30 nm of alumina (Al_2O_3) and was made as follows. The thin film of alumina was deposited on a silicon wafer using an electron beam evaporator at a pressure of 1×10^{-5} torr and at a rate of 60 to 90 nm/min (fig 2.1a). Photolithography was used to pattern the thin film of iron to be deposited. A layer of photoresist AZ 3330-F (from AZ Electronic Materials) was spin cast onto the wafer at 5000 rpm for 60 s (fig 2.1b), baked at 90 °C for 60 s and exposed using a contact aligner with a dosage of 100 mJ/cm^2. The photoresist was then developed with AZ 300 MIF developer (from

13

| a. Al$_2$O$_3$ on Si | b. Photoresist | c. Lithography | d. Deposit Iron |

| e. Lift Off | f. Grow CNTs | g. Knock over CNTs |
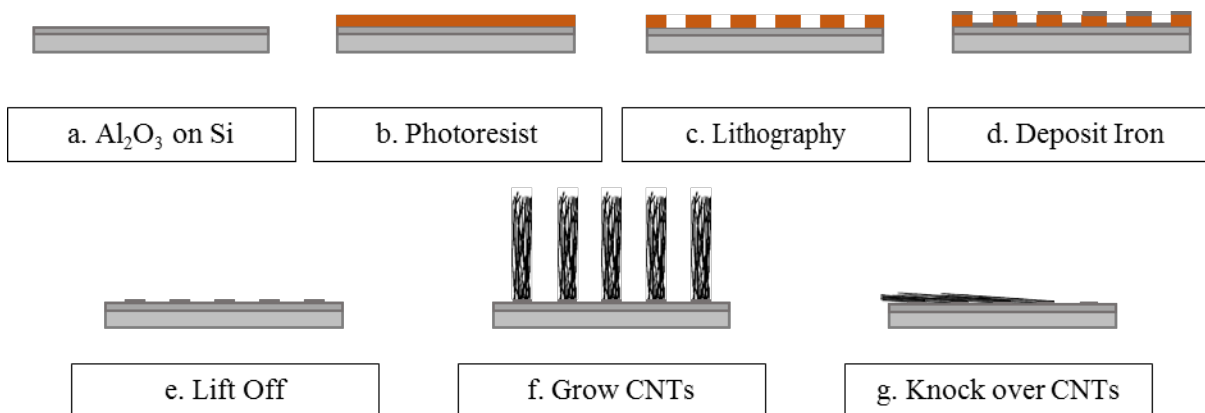
Figure 2.1: The Process diagram for making a CNT sheet. These were the steps to make a CNT sheet from knocked down CNTs. a) A layer of aluminum oxide was deposited on a silicon wafer. b) Photoresist was spin cast onto the wafer. c) The photoresist was lithographically patterned. d) A film of iron was deposited. e) The photoresist was stripped off. f) CNTs were grown on the layer of iron using CVD. g) The CNTs were wetted with IPA and knocked over.

AZ Electronic Materials) for 35 s followed by a 25 s rinse with water and another 60 s bake at 90 °C (fig 2.1c). A 4 nm thick iron film was then deposited on the wafer in a thermal evaporation at a pressure of 1×10^{-5} torr and at a rate of approximately 2.4 nm/min (fig 2.1d). After the iron was deposited, the wafer was sonicated in a bath of N-methyl-2-pyrrolidone (NMP), removing the rest of the photoresist and leaving a patterned iron layer (fig 2.1e). The wafer with alumina and patterned iron was then placed in a 1" quartz tube of an atmospheric CVD system and heated to a temperature of 750 °C while flowing 170 sccm of hydrogen. When the furnace reached 750 °C, 470 sccm of ethylene was added to the hydrogen flow. The growth process lasted approximately 12 min, after which the hydrogen and ethylene were shut off and 20 sccm of argon flowed while the furnace cooled to 200 °C. Upon reaching 200 °C, the samples were removed from the furnace (fig 2.1f).

Knock-down of CNT Forests

At this point, the CNTs in the CNT forest went through a process of densification, which used isopropyl alcohol (IPA) to wick the CNT forest together. [9,37,38] The CNT forest and its

14
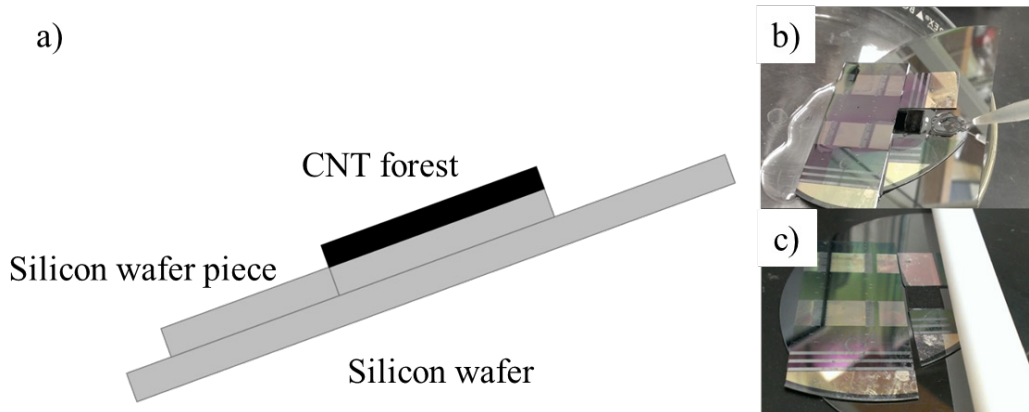
Figure 2.2 a) A representation of the setup to spray the CNT forest with IPA. b) Spraying IPA on the CNT forest. c) Knocking down the CNT forest with a roller. Images taken by Derric Syme.

substrate were placed on another silicon wafer tilted at 20°, with a small wafer piece preventing the CNT forest with its substrate from sliding off (fig 2.2a). A stream of IPA (Fisher Chemical) was aimed above the CNT forest onto the silicon wafer so that the IPA would flow over the CNT forest until it was entirely wetted (fig 2.2b). The wetted CNT forest was then placed on a level surface and a 13 mm diameter PTFE cylinder was rolled over the CNT forest, knocking it down into a thin, aligned CNT sheet (fig 2.1g and fig 2.2c). At this point, the CNT sheets were dried and were left attached to the silicon chip on which they were grown for handling purposes.

Preparing CNT/Polyimide Composite

For polymer impregnation, the CNT sheets were dipped for 15 min into a 1:2 polyimide:N-methyl-2-pyrrolidone (NMP, Sigma-Aldrich) by weight mixture (fig 2.3a). The polyimide was mixed with NMP to lower its viscosity. NMP was added to the polyimide lowering its viscosity and allowing the polyimide to better impregnate the CNT sheets. Impregnated CNT sheets were placed on a hot plate at 100 °C for 30 min and then in a vacuum oven at 85 °C and 75 torr for 60 min.

Silicon wafers were used during hot pressing as polished planar template to create a smooth composite surface. Silicon wafers were perfluorinated to prevent the composites from sticking to the wafers during hot pressing. To perfluorinate silicon wafers, they were placed in a desiccator with approximately 5 mL of a fluorosilane (tridecafluoro-1 1 2 2-tetrahydrooctyl trichlorosilane, Sigma Aldrich). The desiccator was evacuated with a rough vacuum pump for 10 min, sealed, and left under vacuum for 24 hr. Vapor transport of the fluorosilane allows for the functionalization of the silicon wafers. To press the composite, the polished perfluorinated silicon wafer surface was placed in contact with the top surface of the composite, introduced into a hot press, and heated to 180 °C (fig 2.3b). When the temperature reached 180 °C, the pressure was increased to ~11 MPa and held there for 60 min. After 60 min, the heater was shut off and the press cooled to room temperature, then the composite was removed from the press. Following hot pressing, the composites were placed in a vacuum at 1×10^{-5} torr and heated to 400 °C and held there 60 min to cross link the polyimide.

The composites were released from the silicon wafer chips by immersion in 48% hydrofluoric acid (HF HX0621, EMD Millipore) for 5 min. The composites were then rinsed in a DI water bath for 5 min, followed by the two neutralizing baths for 5 min each, each consisting of sodium bicarbonate in DI water, then an additional DI water bath for 5 min (fig 2.3c). Afterward, the composites were placed between two PTFE washers and air dried.

| a. Impregnation | b. Hot Press | c. HF Release |
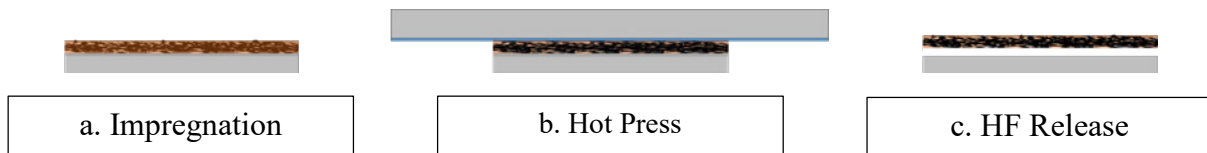
Figure 2.3: Process diagram for making a CNT/polyimide composite. a) A CNT sheet on a silicon wafer is dipped into polyimide. b) The CNT sheet with polyimide is placed against a perfluorinated silicon wafer, hot pressed then cured in a vacuum oven. c) The composite is released with HF acid.
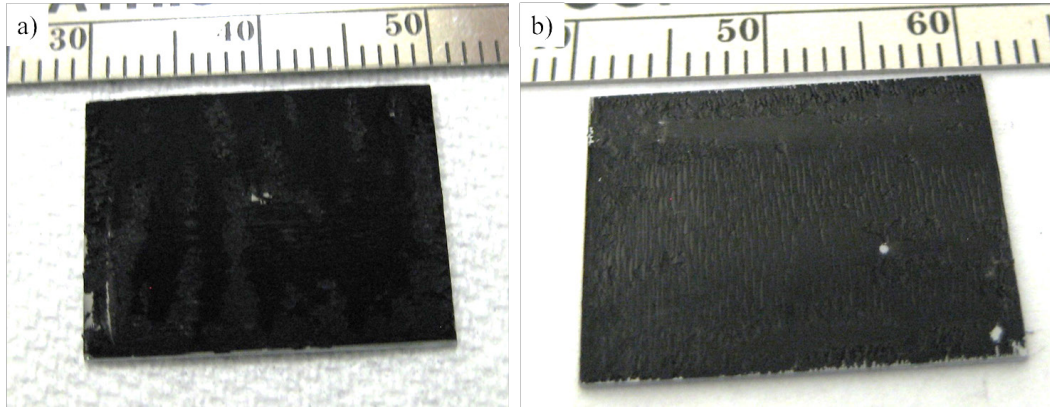
Figure 2.4 Two images of CNT sheets that were sandwich together. a) This sheet was knocked down across the short axis of the wafer chip. b) This sheet was knocked down across the long axis of the wafer chip.

| a. Dual Layer Impregnation | b. Dual Layer Hot Press | c. Dual Layer HF Release |
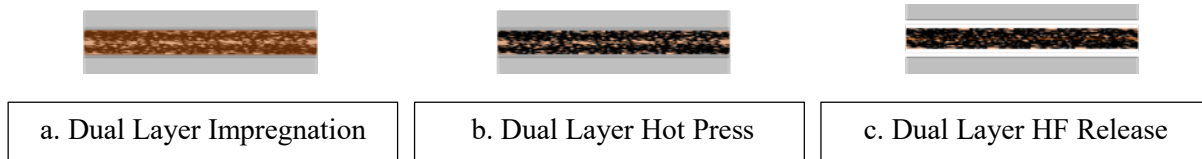
Figure 2.5: Process diagram for making a dual layer CNT/polyimide composite. a) Two CNT sheets on silicon wafers are dipped into polyimide and placed facing each other in the polyimide. b) The CNT/polyimide composite is hot pressed then cured in a vacuum oven. c) The composite is released with HF acid.

Preparing Dual Layer CNT/Polyimide Composites

CNT/polyimide composites were also prepared with two layers of CNT sheets. The CNT alignment in the sheets were oriented perpendicular to each other (fig 2.4). The dual layer composites were made with a similar process as the CNT/polyimide composites with one layer. The main differences occurred during impregnation and hot pressing. Two CNT sheets were dipped in the same polyimide/NMP solution used previously. Before removing the CNT sheets from the solution, the CNT sheets were placed on top of each other sandwiching the two CNT sheets between the silicon wafer chips on which they were grown (fig 2.5a). The NMP was evaporated from the composite in the same manner as detailed in preparing single layer composites.

17

Since the dual layer composites were already sandwiched between the silicon wafer chips there was no need to use perfluorinated wafers. The composites were introduced into a hot press, and heated to 180 °C (fig 2.5b). When the temperature reached 180 °C, the pressure was increased to ~11 MPa and held there for 60 min. After 60 min, the heater was shut off and the press cooled to room temperature before the composite was removed. Following hot pressing, the polyimide was cross linked in a vacuum oven as previously described for single layer composites. Releasing the two layer composites followed the same process as described for single layer composites using HF and subsequent neutralizing and DI water baths (fig 2.5c).

Bulge Testing CNT/Polyimide Composites

The released composites were glued between 2 metal washers using either M-bond 610 adhesive or 3M Super 77 multipurpose adhesive applied to the metal washers (fig 2.6a). The inner diameter of the washers was approximately 4.9 mm. The composites glued into the washers were then secured and tested on a custom bulge tester. The test consisted of applying pressure to the back of the composite in steps and measuring the bulge profile of the composite at each pressure step (fig 2.6b). The bulge profile was measured by a laser displacement (LD)
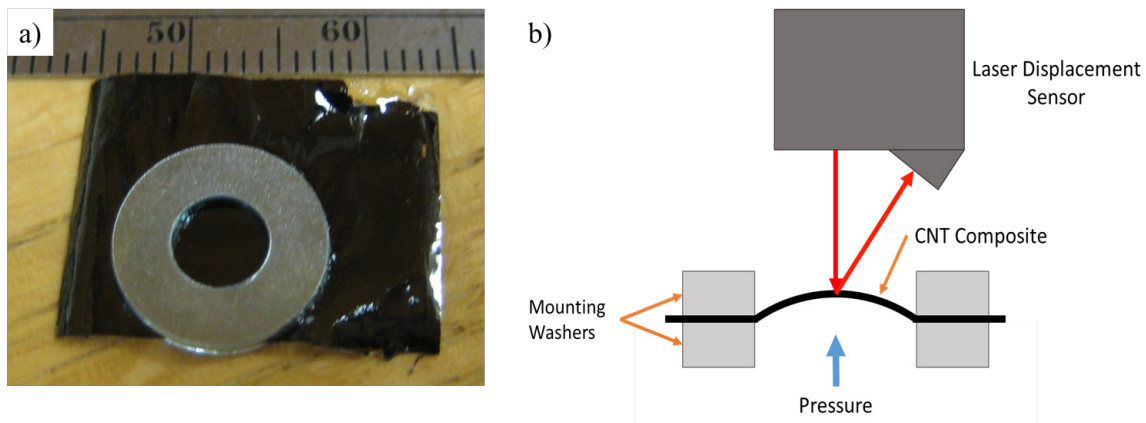
Figure 2.6 a) An image of a CNT/polyimide composite glued between two washers. b) An illustration of the setup of a bulge test. The composite and washers are secured to the base of the bulge tester. During a test, pressure is applied to the underside of the composite causing it to bulge and a laser displacement sensor is scanned across the composite to measure the bulge profile.

18
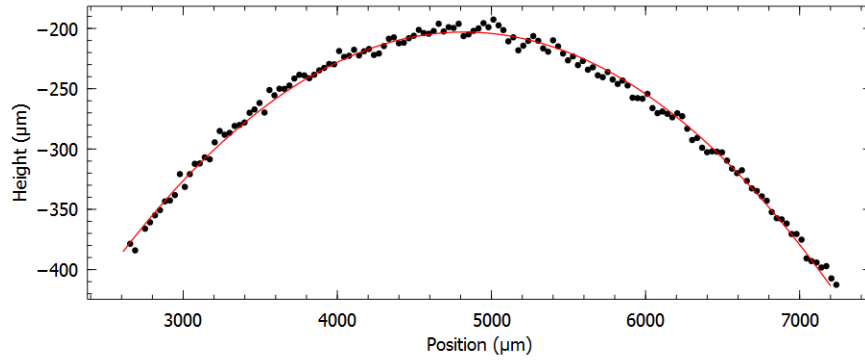
Figure 2.7 The height profile of a bulge of a composite. A circle was fitted to the points in order to calculate the stress and strain in the composite. The line in the plot is a portion of that fitted circle.
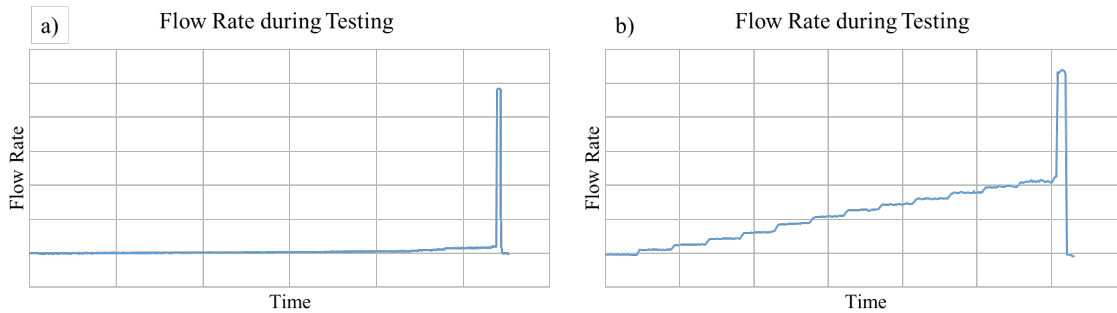
Figure 2.8 a) The flow rate during bugle testing of a composite that did not leak until it burst. b) The flow rate during bulge testing of a composite that was leaking. The steps in the plot correspond to increases in pressure during testing.
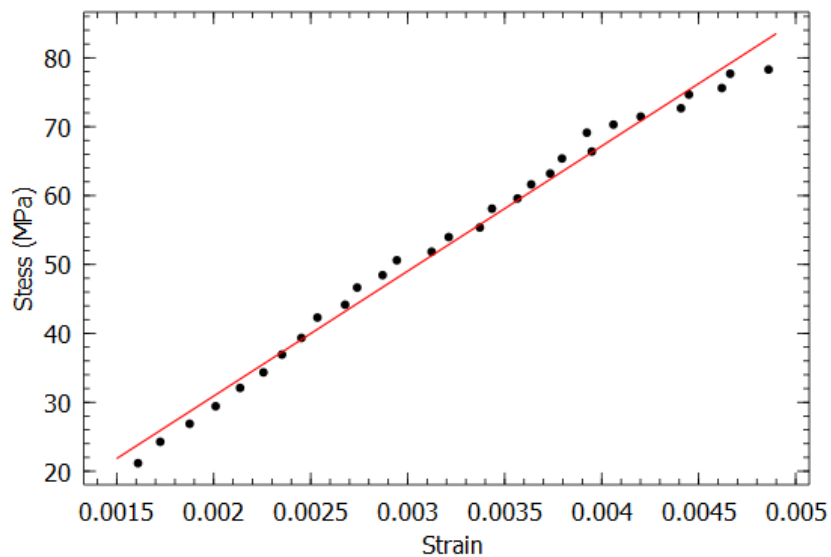
Figure 2.9 A graph of stress vs strain calculated from bulge test data. The solid line is fitted to the slope of the stress strain curve with the slope being the biaxial modulus.

sensor that was scanned in a line across the composite and at the end of each line the pressure was incremented with the scanning repeated. During each line scan, the height of the bulge was recorded as well as the position of the LD sensor, pressure and gas flow. A plot of the bulge profile was made by plotting the position of the LD sensor and the height (fig 2.7). The gas flow was recorded to detect any leaks in the composite and to signal when the composite had burst thereby ending the test. Typical gas flow plots are in figure 2.8. The first plot is of a test where the composite did not leak and the spike on the plot is when the composite failed or burst (fig 2.8a). The second plot in the figure is a test where the composite was leaking and each step corresponds to an increase in pressure (fig 2.8b).

The stress and strain of the composite at each pressure step were extracted by using equations (1) and (2) that were derived by J.J. Vlassak.[43] To use these equations, a circle must be fitted to the bulge profile of the composite. After fitting a circle to the bulge profile, the radius of the circle and the pressure for that line scan were used in equation (1) to calculate the stress in the composite.

$$\sigma = \frac{P * R_c}{2 * t} \tag{1}$$

Where σ is the stress in the composite, P is pressure, R_c is the radius of the fitted circle, and t is the thickness of the composite. The maximum tensile stress of a composite is also known as the tensile strength. The second equation derived by J.J. Vlassak was used to calculate the strain of the composite at each pressure step. The radius of the fitted circle and the inner radius of the washers were used in equation (2) to calculate the strain of the composite.

$$\varepsilon = \frac{\sin^{-1}\left(r_o / R_c\right) - r_o / R_c}{r_o / R_c} \tag{2}$$

Where ε is the strain and r_o is the inner radius of the washers. Plotting stress vs strain (fig 2.9)

and finding the slope of the line will then give the biaxial modulus, which is related to the

Young's modulus by

$$Y(1 - v) = E \qquad\qquad (3)$$

Where Y is the biaxial modulus, v is the Poisson's ratio, and E is the Young's modulus.

Results

A CNT/polyimide composite that has been released from the silicon wafer chip on which

it was grown is shown in figure 2.10. The image is of the front and back of the composite. The

image of the front of the composite shows the repeating line of the knocked over rows and the

image of the back is noticeably smoother than the front because it was in contact with a silicon

wafer chip. A dual layer CNT/polyimide composite is shown in figure 2.11. Both the front and

back of the composite are smooth since it was sandwiched between two silicon wafer chips.

To view the microscopic alignment of the CNTs, SEM images of the knocked down CNT

sheet were taken. The SEM image in figure 2.12a shows that the rows of CNTs in the composite

lay down in the direction of knocking down and that the cross supports folded down between the
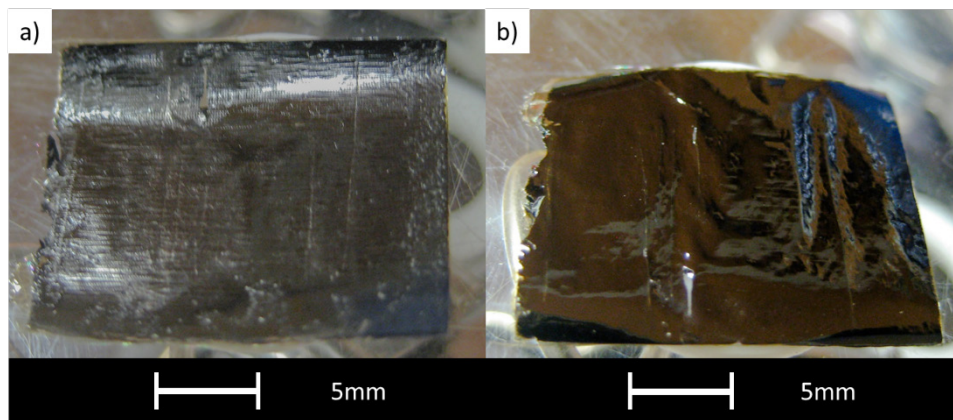
Figure 2.10 Images of the a) front and b) back of a released supported catalyst
composite.
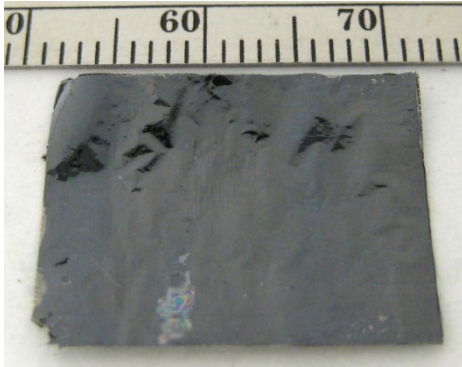
Figure 2.11 An image of a released dual layer composite
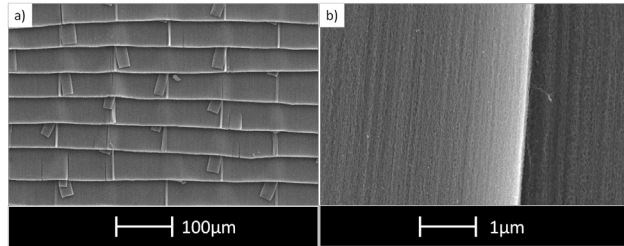
Figure 2.12 a) An SEM image showing the knocked down CNT forest. The pieces of CNT forest scattered are support structures for keeping the forest vertical during growth. b) An SEM image showing the general alignment of the CNTs in the CNT sheet.
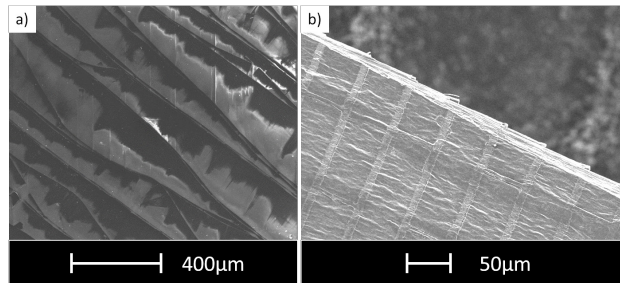
Figure 2.13 a) An SEM image of the CNT/polyimide composite. The overlapping CNT layers is not obvious without the sample charging caused by the thicker areas of polyimide. b) An SEM image of the back of the composite showing the pattern on which the CNTs were grown.
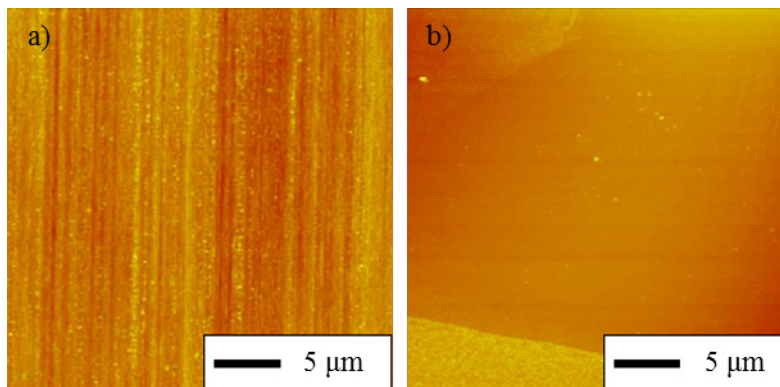
Figure 2.14 AFM images showing the roughness of the a) front and b) back of the composite. The alignment of the CNTs on the front of the composite is in the vertical direction. On the back of the composite the base of the CNT forest is on the bottom left corner of the image in yellow.

CNT layers. Looking at the alignment of CNTs in a layer in figure 2.12b shows the general alignment of those CNTs. An SEM image of a composite shows areas charging. This is where the polyimide is thicker and the CNT sheet is thinner (fig 2.13a). Viewing the back side of the composite in the SEM shows the pattern on which the CNTs were grown and also shows the smoothness of the back of the composite (fig 2.13b). Atomic force microscope (AFM) images were used to quantify the smoothness of the composite. AFM images of the composite in figure 2.14 show the front has a roughness of 29.5 nm over a 30 μm by 30 μm area (fig 2.14a) and the back has a roughness of 14.2 nm over a 20 μm by 20 μm area (fig 2.14b). To see how well the polyimide filled the composite a cross section in the composite was made using a focused ion beam (FIB) on an SEM. The SEM image of the cross section shows no visible voids in the composite (fig 2.15).

In most of the composites produced, defects were present. The defects were most commonly formed during the CNT growth or the knock down processes (fig 2.16). The defects formed during the growth process were from the CNT forest falling over or short to no CNT growth in some areas (fig 2.17). The defects from the knock down process were caused by the layers of CNTs not laying down or sliding before laying down, which resulted in rough areas and nonuniform thicknesses, respectively (fig 2.18a). Looking at these composites in an optical microscope with lighting from the front and the back showed that areas where light was transmitted corresponded to defects in the composite (fig 2.18). A backlight was used in order to see the defects while gluing washers to the composite. The backlight was an array of LEDs covered by paper to diffuse the light (fig 2.19). A defect that was unique to dual layer composites was the separation of the layers of the composite. The delamination is visible in figure 2.20 were the weight of a washer was enough to separate the layers in the composite.

23
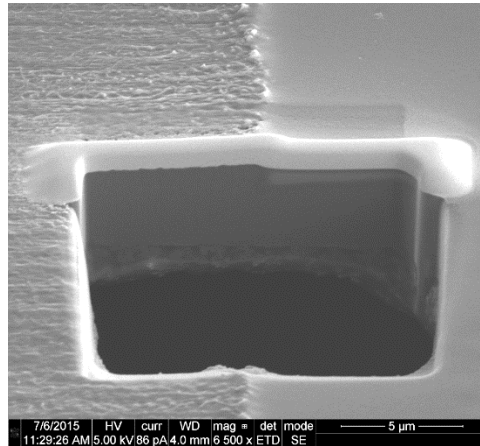
Figure 2.15 An SEM cross section of the composite. No voids are visible at this scale on the face of the cross section.
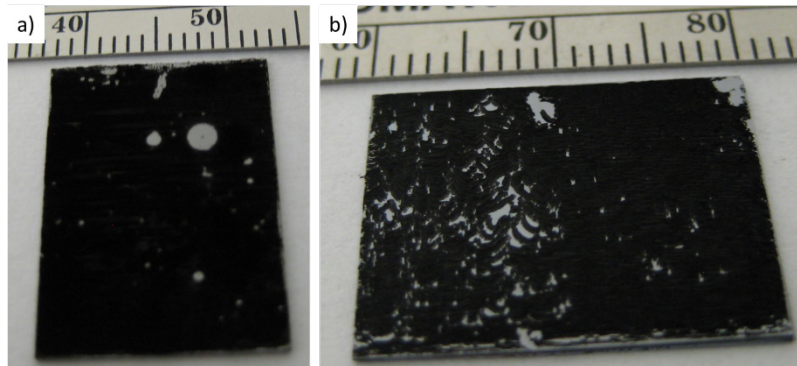
Figure 2.16 a) Growth defects in a CNT forest on a silicon wafer chip. Within the lighter circles no CNT growth took place. b) Defects on the left side of the CNT sheet were from the CNT forest sliding before knocking over.
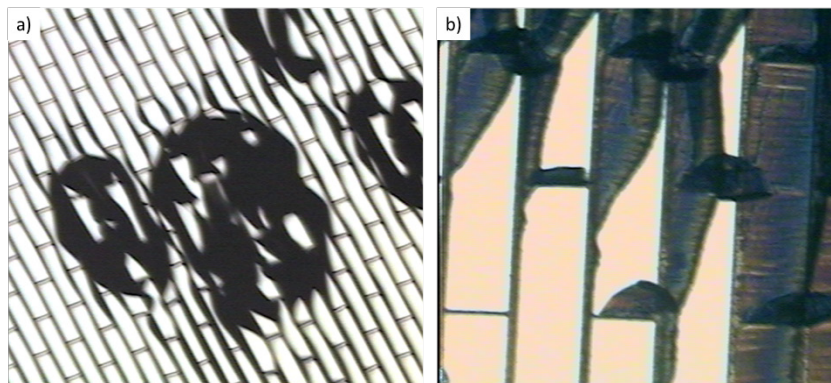
Figure 2.17 Optical microscope images of a) a CNT forest that has partially fallen over, and b) an area in a CNT sheet that had been knocked over where the CNT forest did not grow well leaving gaps between knocked over rows.

24

a)

b)

c)
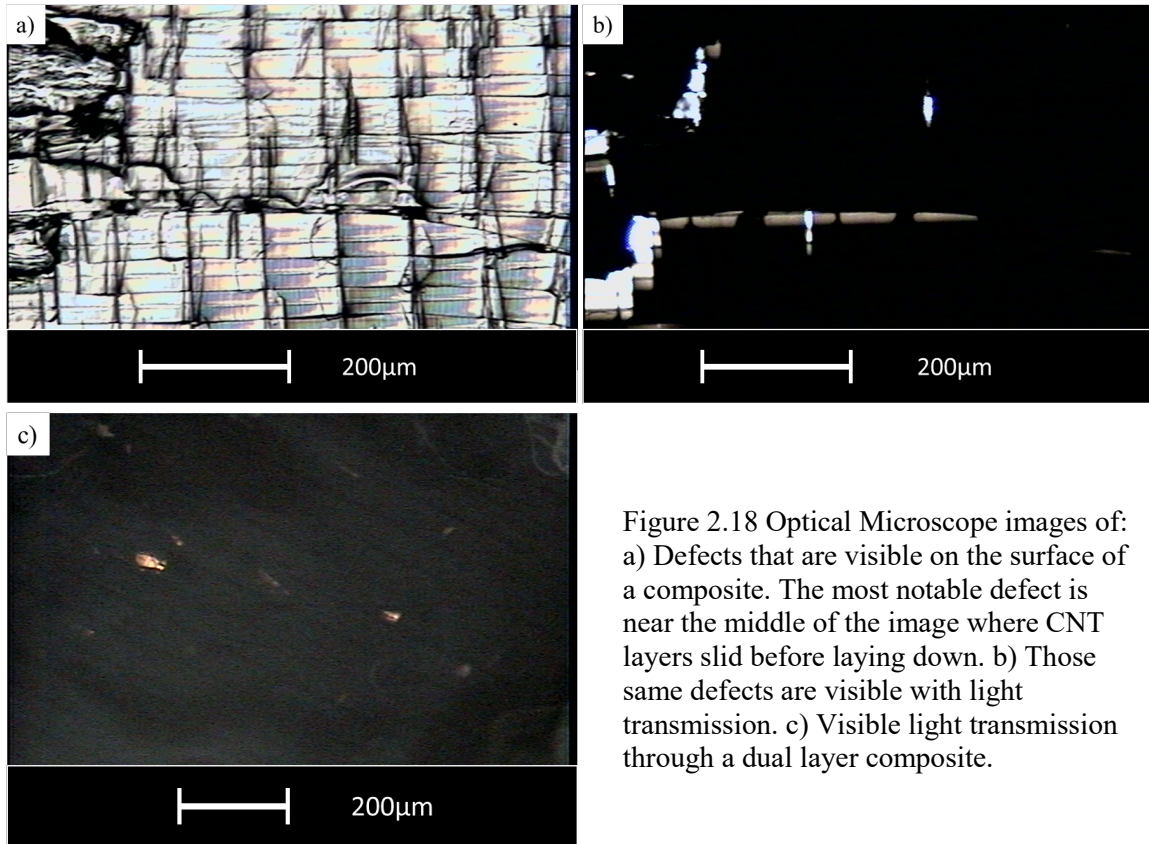
Figure 2.18 Optical Microscope images of: a) Defects that are visible on the surface of a composite. The most notable defect is near the middle of the image where CNT layers slid before laying down. b) Those same defects are visible with light transmission. c) Visible light transmission through a dual layer composite.
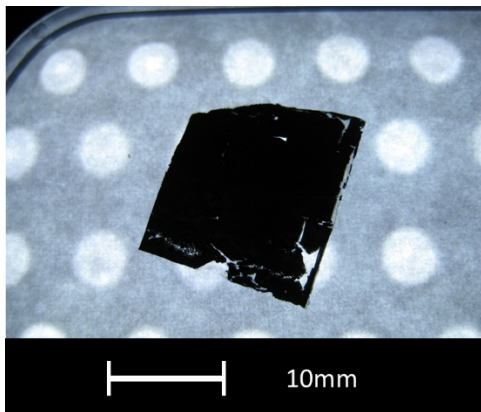
Figure 2.19 Composite on an array of LEDs used for backlighting.

Figure 2.20 Separation of the dual layer composite from the weight of the washer it was glued to after bulge testing.
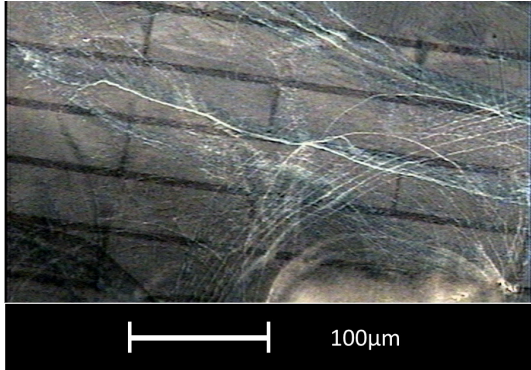
Figure 2.21 An optical microscope image of silver nanoparticles on the back side of the composite.
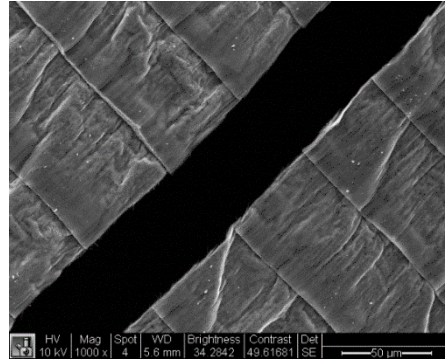
Figure 2.22 The typical failure direction in the composites was parallel to the alignment of the CNTs.

Bulge testing the CNT/polyimide composite presented a challenge as the composites were not initially visible to the LD sensor. The composites were not visible to the LD sensor because the LD sensor required a laser to scatter off the composites to measure the height. The composites reflected the laser rather than allowing it to scatter. Silver nanoparticles were deposited onto the composites so that the laser could be scattered. To deposit the silver nanoparticles, the composites were heated on a hot plate and then approximately 0.25 mL of diluted colloidal silver in water was sprayed with an air brush onto the composite and the water evaporated leaving the silver on the composite (fig 2.21). With silver nanoparticles, the composite scattered the laser enough to be detected.

Bulge testing measured an average burst pressure of 7.67 psi for these composites; for single layer composites the average was 6.47 psi and for dual layer composites the average was 11.29 psi. It was observed that the typical direction of failure was parallel to the alignment of the CNTs (fig 2.22). The tensile strengths of the composites were difficult to determine because the thicknesses of the composites were not constant over areas of testing due to the defects. The backlighting helped in seeing larger defects but there were still many smaller defects that were

26
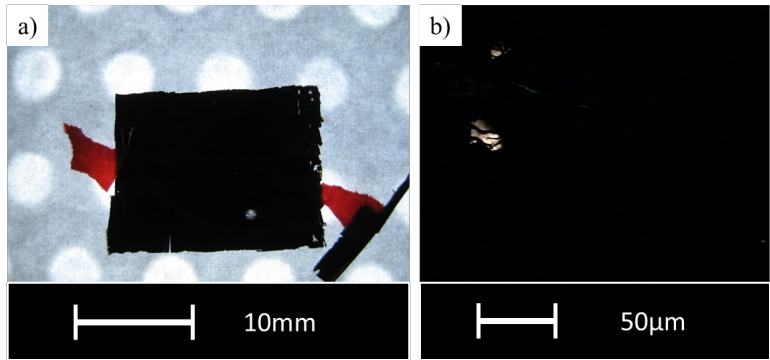
Figure 2.23 a) Composite backlit by LEDs. b) An optical microscope image showing defects in the composite that were not visible without a microscope.
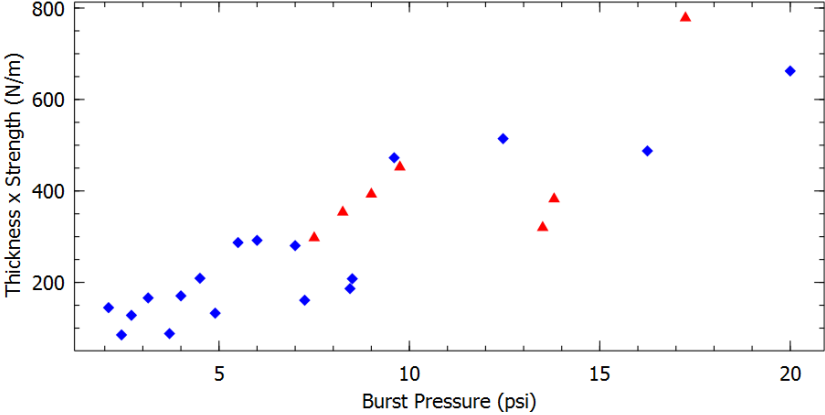
Figure 2.24 The graph shows the rough correlation between burst pressure and thickness multiplied by tensile strength for the composites. The single layer composites are the diamond symbols and the dual layer composites are the triangles.
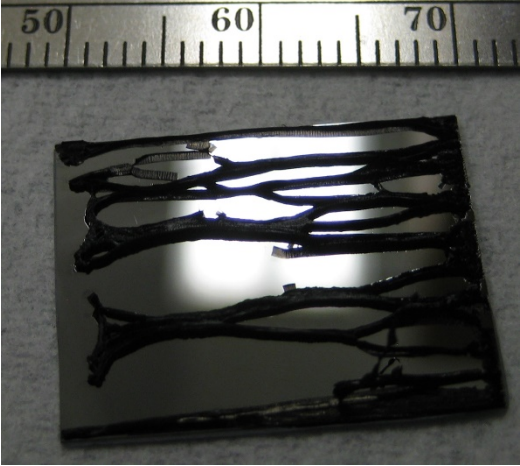
Figure 2.25 A CNT forest that was washed off with IPA

only visible in an optical microscope with backlighting (fig 2.23). Since the tensile strength of a composite could not be determined due to uncertainty in its thickness, the tensile strength multiplied by its thickness was determined. Finding tensile strength multiplied by thickness was done by rearranging J.J. Vlassak's derived equation (1)[43] and solving for tensile stress (σ) and thickness (t).

$$\sigma * t = \frac{1}{2} * P * R_c \qquad\qquad (4)$$

The average tensile strength multiplied by thickness was 293 N/m for all of the composites; for single layer composites the average was 242 N/m and for dual layer composites the average was 425 N/m. Thickness multiplied by tensile strength versus burst pressure is plotted in figure 2.24 for each composite.

Discussion

Defects in the composites were one of the reasons why the composites were not as strong as anticipated. The defects, as stated earlier, appeared during the CNT growth or the knock down processes. The CNT growth was not consistent in height and straightness, as was seen in figure 2.17. The range of CNT forest heights was possibly caused by contamination on the wafer before growth or gas variation in growth. The defects from the knock down process occurred from the PTFE cylinder slipping instead of rolling, IPA washing the CNTs off the wafer, or the CNTs sliding then knocking over (fig 2.16b and fig 2.25). The PTFE cylinder slipping was caused by human error, while the other two were caused by having poor adhesion of the CNT forest to the wafer. The CNT forest seemed to adhere better to the wafer when the ratio of ethylene gas to hydrogen gas was higher during the growth process.

Bulge testing was another reason why the composites were not as strong as expected. The bulge testing probes the strength of the composites in all directions at the same time, parallel with the CNTs, the stronger direction, and perpendicular to the CNTs, the weaker direction. This results in lower strengths and burst pressures for the composites. In bulge testing, it must also be noted that equations 1-3 require some assumptions in order to be derived and to calculate material properties. The assumptions are that the film being tested is flat, has no residual stresses, does not slip in between the washers, and is isotropic and homogeneous, or the same in every direction. These composites, in particular, do not satisfy the last condition because the CNTs are aligned in one direction for single layer composites or 2 directions for the dual layer composites. The composites could be pull tested to probe the strength in one dimension, but the strength may not be calculable until the composites are free of defects.

The material properties of the composites were difficult to determine because of defects and the assumptions made by bulge testing. In equation (1), the thickness of the composite is used to calculate the strength of the composite but the thickness of the composite is difficult to measure due to the defects. The defects made composites thicker in some areas and thinner in other areas leading to multiple thicknesses. The Young's modulus is also unable to be determined since it is coupled to stress through the slope of the stress vs strain line. The tensile strength multiplied by the thickness, as in equation (4), is the closest strength that could be calculated for these composites with variable thicknesses. The graph in figure 2.24 summarizes the bulge test results by plotting the relation between burst pressures and tensile strength multiplied by thickness.

The results for the dual layer CNT/polyimide composites show that they did not burst at any higher pressure than the single layer composites. The composites were weak due to the layers not staying adhered together and defects in the individual layers.

Conclusion

In this research, making CNT/polyimide composites with aligned CNTs has not shown much promise in becoming a high strength composite, but research of others has shown that composites made from CNT sheets with aligned CNTs have had strengths of 100s of megapascals.[21] The work for this project going forward would be to increase the yield of defect free CNT sheets. To create defect free CNT sheets, the CNT growth and knock down processes would need to be improved. The CNT growth process could be improved by limiting contaminates in the growth and adjusting the hydrogen to ethylene flow ratio leading to growing CNT forests that are more uniform and better attached to the silicon chip. Eliminating the human variation when the PTFE tube is rolled over the CNT forest could be done by making the roller mechanically driven by a computer or by using a technique shown in other research to knock over CNT forests with a shear force.[21] Implementing these changes to the process and fine tuning the growth of the CNTs should improve the strength of the supported catalyst CNT/polyimide composites.

Chapter 3
Microfabrication of Carbon Nanotube Composite Structures by Etching

Introduction

As stated in the background section, the strong composites made by Cheng et al., Wang et al., and Liu et al. are interesting as a micromechanical structure because their tensile strengths were between 3.1 GPa and 4.5 GPa and their Young's moduli were between 275 GPa and 295 GPa. The strengths of these composites are comparable to that of crystalline silicon (ranging from 1 GPa to 7 GPa[31,32]) and the Young's moduli of these composites are much greater than that of crystalline silicon (which is between 50 GPa and 190 GPa[33]). To be able to include these high strength CNT/polymer composites into MEMS, the composites (CNTs and polymer) need to be able to be patterned. In order for a composite to be patterned it needs to be smooth enough to use photolithography and it needs to be able to be selectively removed.

One method that researchers have used to pattern CNTs is an oxygen plasma etch. Lu et al.[8] and Behnam et al.[36] made buckypaper using a process of filtering CNTs out of a solution. Using this process of filtration, each group was able control the thickness of the films. The CNT films were etched using an oxygen plasma in an inductively coupled plasma reactive ion etcher (ICP RIE). Lu et al. used photoresists AZ5214 and AZ4620 to protect parts of the CNT films from etching. They determined that AZ5214 at ~1.5 μm thick was thick enough to pattern CNT films up to 460 nm and AZ4620 was thick enough to pattern their thickest CNT films of 780 nm. The etch rate for their CNT film was about 240 nm/min. Behnam et al. compared the effectiveness of photoresists polymethylmethacrylate (PMMA), LOR3B, and S1813 in resisting etching. Under specific conditions, they found that only S1813 was etched slower than the CNT film and even then it was only etched 25.8 nm/min slower. Yoo et al.[22] created a CNT/polyimide composite by mixing a dry CNT powder with polyimide and then spun the solution onto a substrate and cured the polyimide. After the CNT/polyimide film was cured, photoresist was

used as the mask while the CNT/polyimide composite was patterned using an oxygen plasma etch in an ICP RIE system.

Two of the differences between the research into high strength composites and the research into MEMS composites are the thickness of the composites or films and the CNT density in composites. In the research of Lu et al.[8] and Behnam et al.[36], the thicknesses of the CNT films were all less than 1 μm, compared to the 60 μm thick composite used in the research of Cheng et al.[16] In the research of Yoo et al.[22], the thickness of the CNT/polyimide composite was not stated, but the weight percent of CNTs in the composite was 0.4 wt%, which is really small in comparison to 50 wt% or more of CNTs in composites from the research of Cheng et al.[16], Wang et al.[17], and Liu et al.[18] In these examples of patterning CNT films/composites, photoresist was thick enough to pattern these films, however, to pattern the high strength composites the mask would have to be etched slower than the composite.

In this work we demonstrate a method to fabricate and pattern smooth, thin CNT/polyimide composites, made from CNTs grown by floating or supported catalyst CVD, using a hard mask of silicon nitride during an oxygen plasma etch. CNT sheets of randomly oriented CNTs, grown by floating catalyst CVD, were impregnated with polyimide. The CNT/polyimide composites were then smoothed by a heated press, followed by curing the polyimide in a vacuum oven. An etch mask of amorphous silicon nitride was deposited on the CNT/polyimide composites to protect parts of it during an oxygen plasma etch. The oxygen plasma etch removed the unprotected portions of the CNT/polyimide composite, leaving the smooth, patterned CNT/polyimide composite.

Process

Etching a CNT composite consisted of two main parts. The first was making the CNT composite by impregnating a floating catalyst CNT sheet (Nanocomp Technologies Inc.) with

32

polyimide (PI-2610 produced by HD MicroSystems), hot pressing against polished silicon

wafers, and curing the polyimide. The second part was depositing a film of silicon nitride in a

PECVD system, the silicon nitride photolithographically patterned in an RIE. With the silicon

nitride hard mask, the CNT/polyimide composite was etched in an ICP RIE.

Preparing CNT/Polyimide Composites

The CNT sheets (fig 3.1a) were processed into composites as follows: the CNT sheets

were dipped for 15 min into 1:2 polyimide:N-Methyl-2-pyrrolidone (NMP) mixture (fig 3.1b).

NMP was mixed into the polyimide to lower its viscosity. The NMP was evaporated from the

composite on a hot plate at 100 °C for 30 min and then in a vacuum oven at 85 °C and 75 torr for

60 min.

Silicon wafers were used during hot pressing as polished planar template to create a

smooth composite surface. Silicon wafers were perfluorinated to prevent the composites from
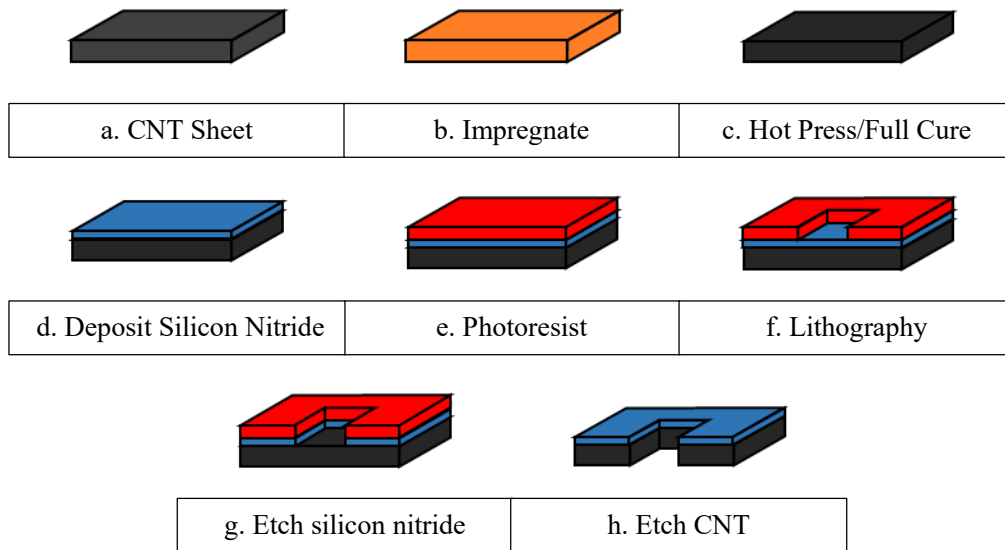
Figure 3.1: Process diagram for making and patterning a CNT/polyimide composite sheet. a) A
CNT sheet. b) CNT sheet impregnated with polyimide. c) CNT sheet with polyimide hot
pressed and cured to make a CNT/polyimide composite. d) A layer of silicon nitride is
deposited onto composite. e) Photoresist is spun on top of the layer of silicon nitride. f)
Photoresist is patterned and developed using photolithography. g) Exposed silicon nitride is
etched away with carbon tetrafluoride. h) Exposed CNT/polyimide composite is etched with an

33

sticking to the wafers during hot pressing. To perfluorinate silicon wafers, they were placed in a desiccator with approximately 5 mL of a fluorosilane (tridecafluoro-1 1 2 2-tetrahydrooctyl trichlorosilane, Sigma Aldrich). The desiccator was evacuated with a rough vacuum pump for 10 min, sealed, and left under vacuum for 24 hr. Vapor transport of the fluorosilane allows for the functionalization of the silicon wafers. To press the composites, the composites were sandwiched between two polished perfluorinated silicon wafers, introduced into a hot press, and heated to 180 °C. When the temperature reached 180 °C, the pressure was increased to ~11 MPa and held there for 60 min. After 60 min, the heater was shut off and the press cooled to room temperature, then the composite was removed from the press. Following hot pressing, the composites were placed in a vacuum at 1×10^{-5} torr and heated to 400 °C and held there 60 min to cross link the polyimide (fig. 3.1c).

Microfabrication of CNT/Polyimide Composites

Both floating catalyst composites and supported catalyst composites were photolithographically patterned. A film of silicon nitride was deposited on top of the composites using a PECVD system (fig 3.1d). The silicon nitride was approximately 400 nm thick. The composites were then bonded to a silicon wafer using photoresist (AZ 3330-F) for handling and to be a thermal contact for temperature control during etching. Next, a layer of photoresist was spin cast at 5000 rpm for 60 s onto the composite, baked at 90 °C for 60 s (fig 3.1e) and exposed using a contact aligner with a dose of 100 mJ/cm^2. The photoresist was then developed with AZ 300 MIF developer for 35 s, rinsed with water for 25 s and baked again at 90 °C for 60 s (fig 3.1f). The exposed silicon nitride film was then etched with a CF$_4$ plasma in a reactive ion etching system (RIE, fig 3.1g), and at a power of 300 W, a CF$_4$ flow rate of 25 sccm, and a pressure of 100 mtorr for 15 min. The final step of the process was etching the composite with an oxygen plasma etch in an inductively couple plasma (ICP) RIE system (Mesc Multiplex

34

Inductively Coupled Plasma V2, Surface Technology Systems, fig 3.1h). The etch in the ICP RIE was done at a pressure of 50 mtorr, an O_2 flow of 55 sccm, 800 W of power on the coil, and power on the platen initially at 100 W (table 1).

The etch rates of the composites were determined by measuring the step height between the etched portion of the composite and the silicon nitride mask in either a scanning electron microscope (S-FEG XL30 FEI or FEI Helios Nanolab 600 DualBeam FIB/SEM) or a 3D profilometer (3D profilometer Zeta 20) and subtracting the approximate silicon nitride thickness. The etch rate of the silicon nitride was determined by depositing it onto a silicon wafer and measuring the thickness of the film with ellipsometry (J.A. Woollam Co., Inc. M-2000DI) before and after etching. To see the internal structure of the composites, cross sections were made using a focused ion beam (FIB) on an SEM. Surface topography of the composites was measured using an atomic force microscope (AFM, Digital Instruments Dimension 5 AFM). AFM was used to measure the effectiveness of hot pressing the composites against polished silicon wafers to minimize roughness.

Results

CNT/Polyimide Composite Sheets

An optical image of a floating catalyst CNT/polyimide composite is shown in figure 3.2a. RMS roughness of the floating catalyst composite was 61 nm over an area of 20 μm by 20 μm (fig 3.3a). Using a micrometer, the average thickness of floating catalyst composites was measured to be 25.6 μm with thicknesses between 21 and 29 μm. Before hot pressing, the average thickness of floating catalyst CNT sheets was 31.4 μm with thicknesses between 28 and 36 μm. This shows the CNT composite sheets were compressed approximately 5.8 μm by hot
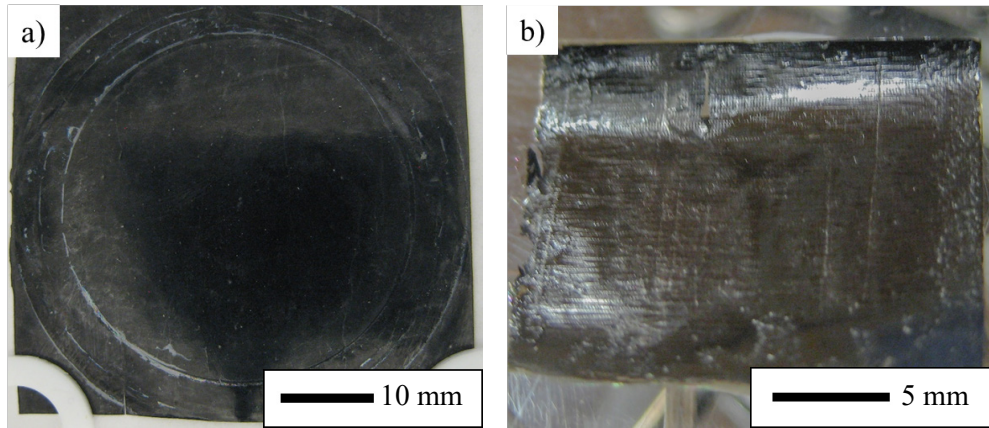
Figure 3.2 Cured CNT/polyimide composites. a) A floating catalyst CNT/polyimide composite. The composite is black because of the CNTs and the circle on the composite is from the clamps that were used to handle the sheet during impregnation. b) A supported catalyst composite
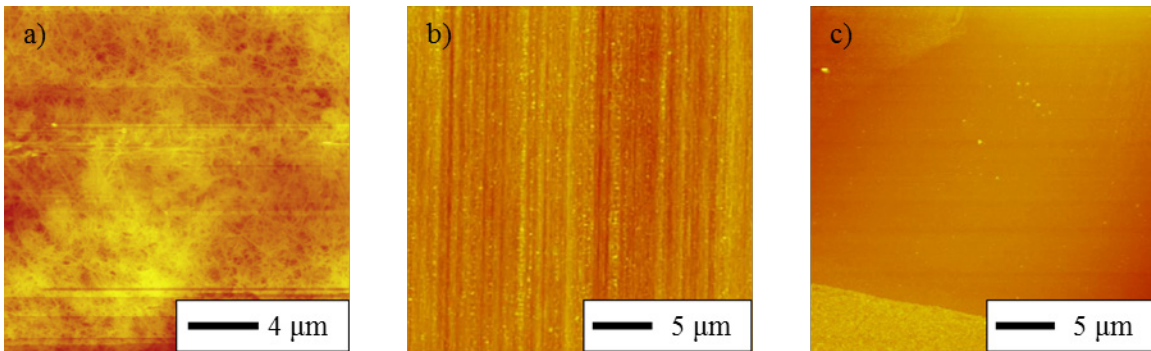
Figure 3.3 AFM images of a floating catalyst composite and a supported catalyst composite. a) 20 μm x 7 μm area of a floating catalyst composite. b, c) 30 μm x 30 μm areas of the front and back of a supported catalyst composite.
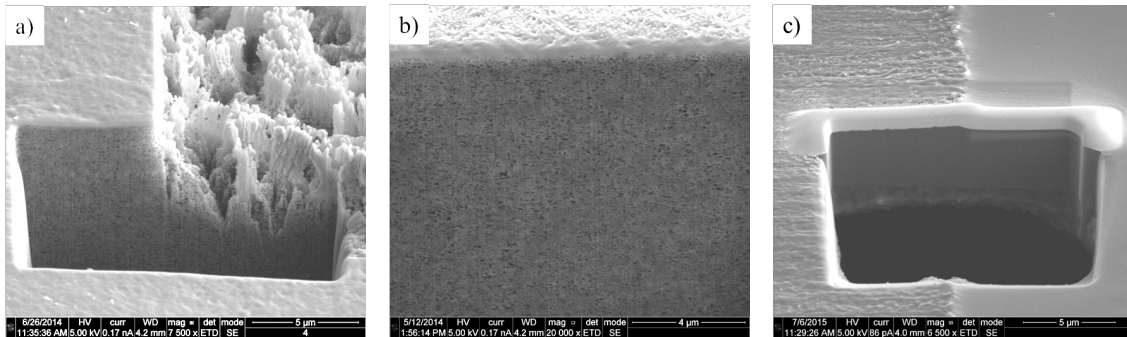
Figure 3.4 SEM images of cross sections into floating and supported catalyst composites. a) A cross section shows nanoscale voids present in the composite and the morphology of oxygen etching a floating catalyst composite. b) A cross section of a different floating catalyst composite also showing voids. c) A cross section of a supported catalyst composite showing no voids on this scale.

36

pressing. The floating catalyst composites had a CNT density of about 85 wt%. The SEM

image of a cross section of a floating catalyst composite shows the presence of nanoscale voids

(fig. 3.4a and 3.4b).

An optical image of the front of a supported catalyst CNT/polyimide composite is shown

in figure 3.2b. The fronts of the supported catalyst composites are the sides of the composites that

were not in contact with the growth wafer, while the backs of supported catalyst composites were

in contact with the growth wafer until release. RMS roughness of the front of a supported catalyst

composite was 29.4 nm over an area of 30 μm by 30 μm (fig 3.3b). The AFM image in figure 3d

shows the roughness on one row of CNTs, but does not show step height between rows on the

front of the composite (fig 2.4c). The step height varied in depending on how well the polyimide

filled in the step. The maximum step height was approximately 1.5 μm. RMS roughness of the

back of a supported catalyst composite 14.2 nm over an area of 20 μm by 20 μm. Using SEM

images, the average thickness of supported catalyst composites was measured to be 6.7 μm with

thickness between 2 μm and 15 μm. An SEM image of a cross section of a supported catalyst

composite does not show the presence of voids on this scale (fig 3.4c).

Etching Silicon Nitride Film

The result of patterning the silicon nitride mask with CF_4 is shown in figure 3.5.

Photoresist that was used to protect parts of the silicon nitride film is shown in the top and

bottom of the image. The middle of the image shows the area where the silicon nitride mask was

exposed to and etched by CF_4. The silicon nitride film 400 nm thick was completely etched

through in 15 min, with the etching parameters as discussed in the process section.
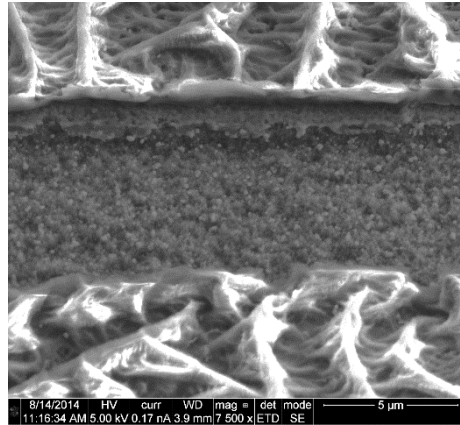
Figure 3.5 SEM image taken after the silicon nitride mask had been etched. Photoresist is visible in the top and bottom of the image. In the middle of the image is where the silicon nitride was etched away, exposing the composite underneath.
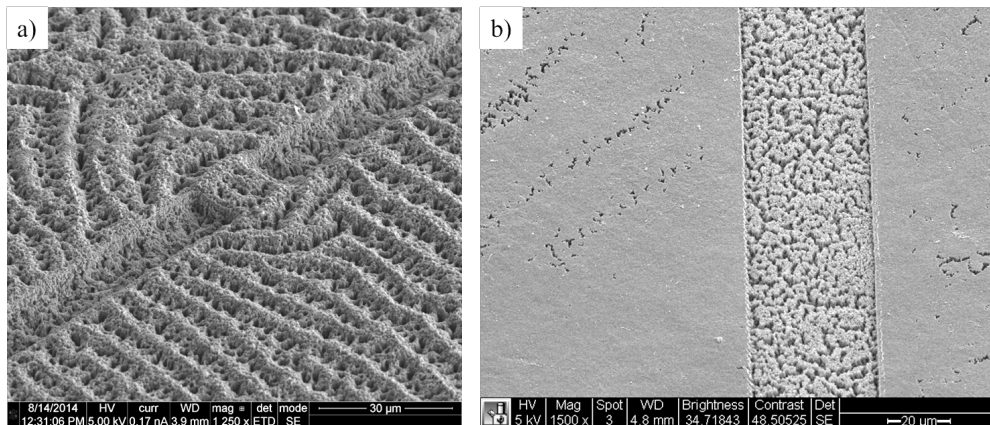
Figure 3.6 SEM images showing the condition of the silicon nitride mask on floating catalyst composites that had been etched with oxygen. a) An image showing a composite with its silicon nitride mask completely etched away. b) An image showing silicon nitride that was damaged during the etch.

To determine whether silicon nitride would be an adequate mask during the oxygen plasma etch the etch rate of silicon nitride was measured. A 355 nm film of silicon nitride was deposited onto a silicon wafer. After etching the silicon nitride for 15 min with 100 W on the platen and the same conditions as mentioned in the experimental section, the thickness of the silicon nitride film was reduced to 57 nm. The etch rate of the silicon nitride mask was approximately 20 nm/min. After etching for 20 min, the silicon nitride mask on a floating
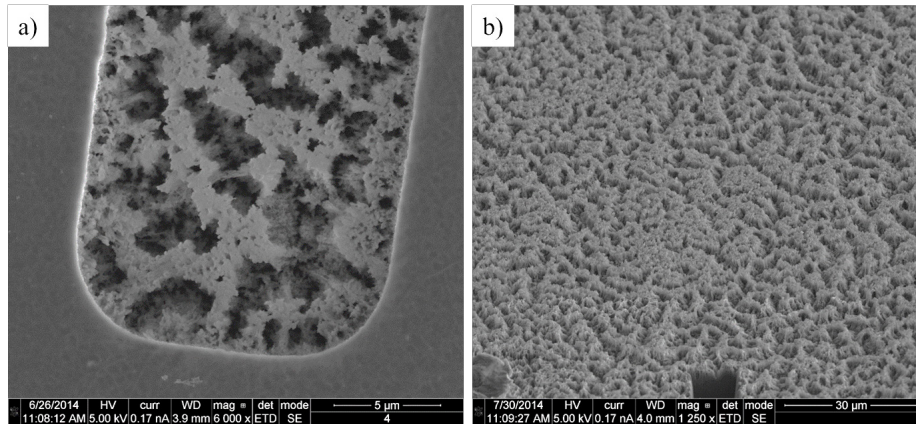
Figure 3.7 SEM images of composites after being etched with an oxygen plasma. a) A composite that had a silicon nitride mask. b) A composite that was etched without a silicon nitride mask.

Figure 3.8 SEM images showing composites after oxygen plasma etch. a) A composite with a silicon nitride mask. b) A composite without a silicon nitride mask. c) A tilted view of an etched composite showing the morphology of the etched structures. d) A cross section showing the height of the structures.

catalyst composite was completely etched away (fig 3.6a). The etch rate of silicon nitride was influenced by the high power used on the platen and the residual fluorine in the ICP RIE chamber.

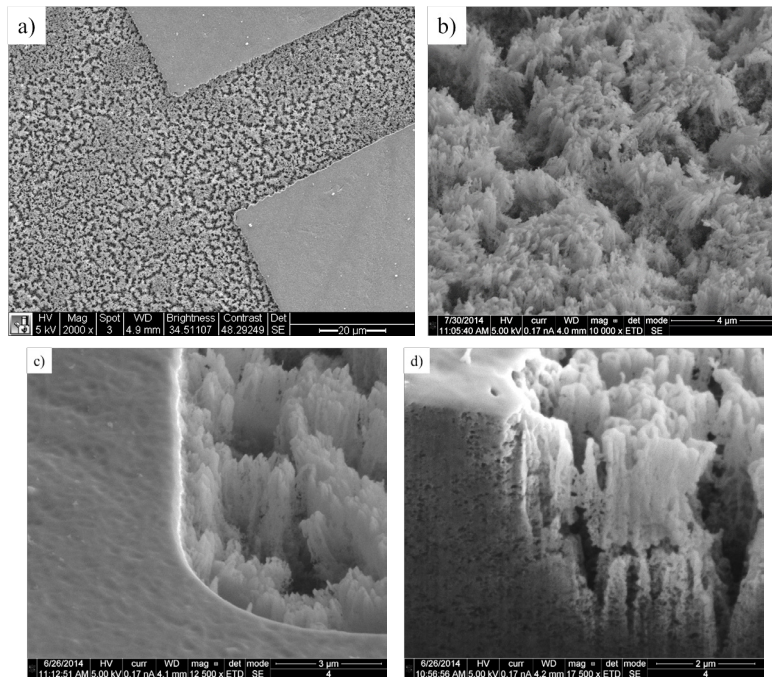The power on the platen was adjusted from 100 W down to 30 W (table 1) and the residual fluorine in the system was reduced by cleaning the chamber for 2 hr before etching the composite. The chamber was cleaned with an oxygen plasma with 800 W on the coil and 100 W on the platen at a pressure of 50 mtorr and with an oxygen flow rate of 55 sccm. By decreasing the platen power to 30 W and reducing the amount of residual fluorine in the chamber, the etch rate of a film of silicon nitride was between 2 nm/min and 5 nm/min. Even with the reduced etch rate of silicon nitride, some 400 nm thick silicon nitride masks were compromised within 5 min of etching (see fig 3.6b).

Etching Floating Catalyst Composites

A floating catalyst composite examined after the oxygen plasma etch revealed that the composite was not etched uniformly (fig 3.7). Micro-structures were present after the oxygen plasma etching in the etched portions of composites with and without a silicon nitride mask (fig 3.7) and were typically more than 1μm tall (fig 3.8d). After etching a floating catalyst CNT/polyimide composite for 20 min, the depth of the etch was measured to be about 1.8 μm, while a composite that was etched for 40 min had an etch depth of about 1.8 μm. The reduction in etch rate with time indicates the possible presence of a contaminate layer.

Performing energy dispersive x-ray spectroscopy (EDX) on floating catalyst composites and CNT sheets revealed the presence of iron (fig 3.9). EDX measured the iron concentration was approximately 10 wt% for CNT sheets and a composite that had been etched for 40 min. A
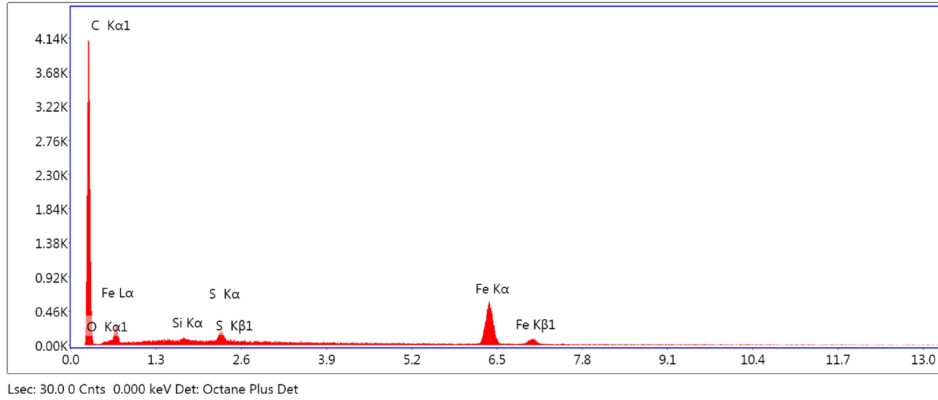
Figure 3.9 An x-ray spectrum of a composite showing that it is contaminated with iron. The iron is residual growth catalyst from CNT growth using floating catalyst CVD.
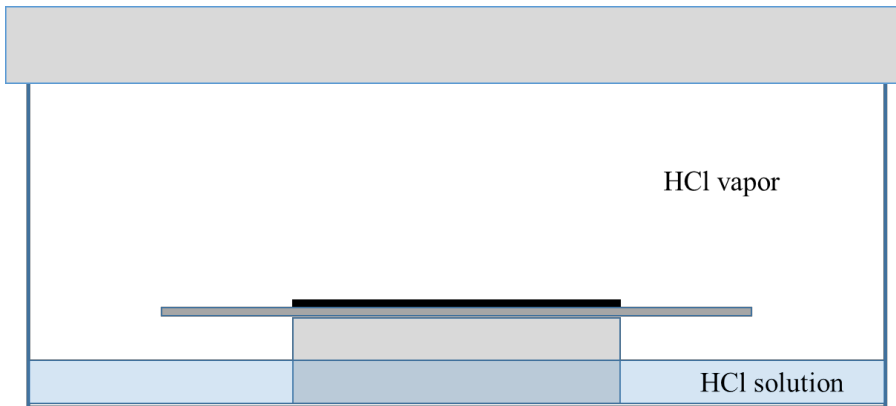
Figure 3.10 An illustration of etching a floating catalyst composite using HCl vapor. The composite is held above HCl solution on a wafer which is on a stand.
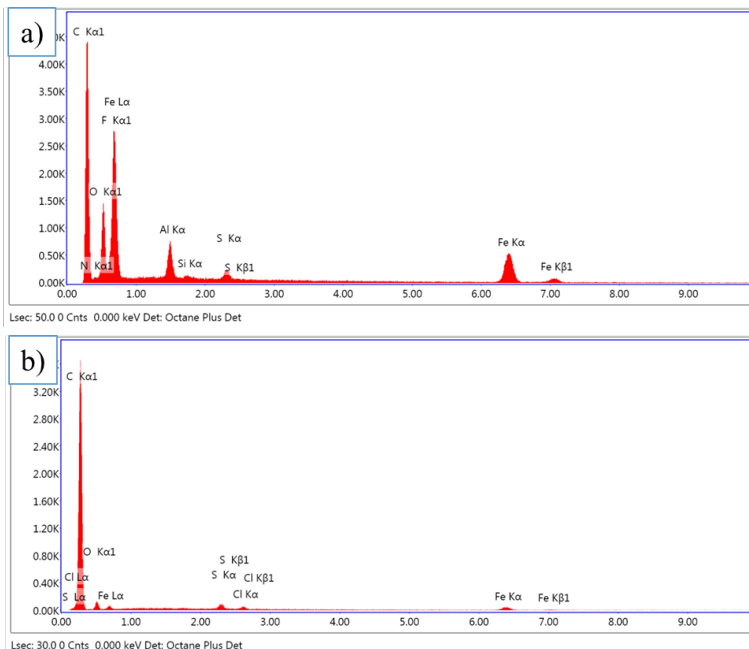
Figure 3.11 a) An x-ray spectrum of a composite before being exposed to HCl vapor. Notice the prominence of the iron peaks. b) An x-ray spectrum of a composite after being exposed to HCl vapor for 2 hr. The iron peaks significantly decreased (approximately 7 wt%).

41
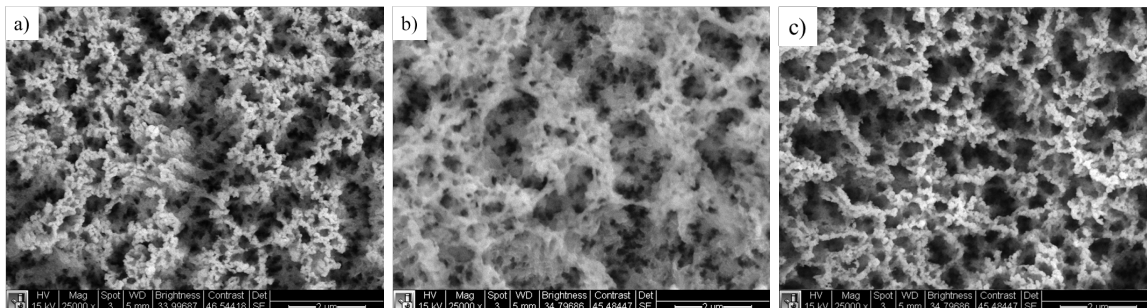
Figure 3.12 SEM images showing a floating catalyst composite after several etches. a) After 40 min of etching with an oxygen plasma. b) After 40min of oxygen etching, 2 hr of HCl exposure and water rinse. c) After an additional 40 min of oxygen plasma etching.
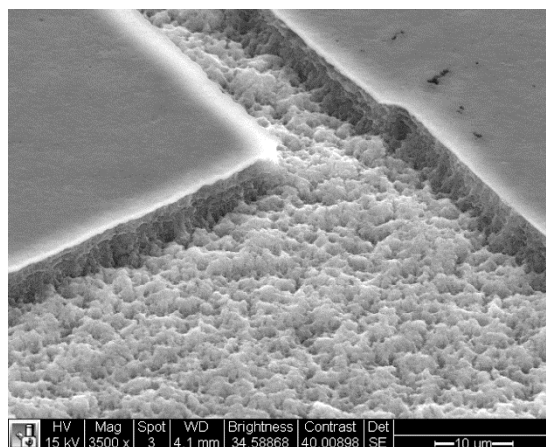
Figure 3.13 An SEM image of a composite that was etched with oxygen for 20 min, then with HCl vapor for 2 hr, then with oxygen again for 20 min.
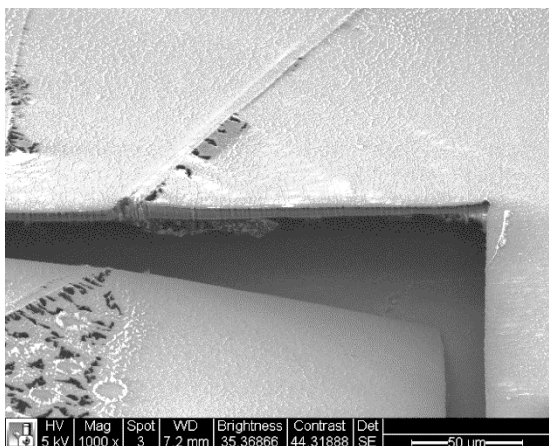
Figure 3.14 An SEM image of a supported catalyst composite that was etched with oxygen for 20 min.
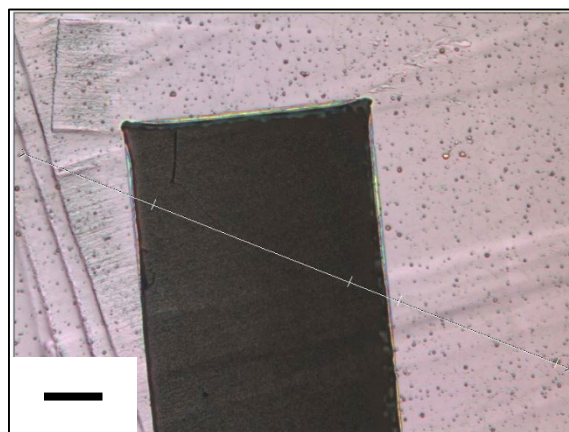
Figure 3.15 Optical microscope image of a supported catalyst composite after 5 min of oxygen plasma etching. The line near the middle of the sample is where the height profile was measured. The scale bar is 20 μm.

composite that was previously etched with oxygen for 40 min was exposed to HCl vapors for 2 hr then rinsed with water (fig 3.10). EDX showed that the iron content near the surface decreased to 2.7 wt% (fig 3.11). Figure 3.12a shows the micro-structures on the floating catalyst composite after 40 min of oxygen plasma etching. Figure 3.12b show the micro-structures on the same composite after the HCl process. After the HCl process and etching for another 20 min, the etch depth of the composite was measured to be about 5.3 μm, which is an additional 3.5 μm (fig 3.13). The composite was etched again for another 20 min and the etch depth gained an additional 0.5μm (fig 3.12c). EDX on that composite then showed that the iron contamination near the newly etched surface was 15.2 wt%, which is a higher concentration of iron than before the previous oxygen etch.

Since the etch rate for floating catalyst composites decreased with time during oxygen plasma etching only an average etch rate can be calculated. During the first 20 min of etching, the average etch rate of a composite was 90 nm/min. After the same composite went through the HCl process, the average etch rate for the composite was 150 nm/min during 20 min of additional etching. The average etch rate for a composite, after it had been etched for 40min and went through the HCl process, was 175 nm/min during 20 min of additional etching. The etch selectivity between the composite and the silicon nitride mask, which had an etch rate of 4.11 nm/min, varied between 22:1 composite:silicon nitride and 42:1 composite:silicon nitride.

Etching Supported Catalyst Composites

The supported catalyst CNT/polyimide composites were etched using the final etch conditions. The supported catalyst composites were completely etched through in 20 min (fig 3.14). The silicon nitride mask for the composite was also compromised in some areas during

the same etch (fig 3.14). The oxygen plasma etch time was then decreased to 5 min.   Etching

the composite for the 5 min gave an average etch depth that was 3.2 μm, which was an average

etch rate of 640 nm/min (fig 3.15). The etch selectivity for supported catalyst composites and

the silicon nitride mask was 155:1 composite:silicon nitride. EDX analysis on supported catalyst

composites did not detect any iron. The conditions for all of the etching parameters are

summarized in table 1.

Table – 1 A Summary of the Plasma Etches used during Processing of the CNT/polyimide Composites.

Etch	Machine	Mask	Gas	Pressure	Power		Material Etch Rate	Mask Etch Rate
					Coil	Platen		
Silicon Nitride	RIE	Photoresist	CF_4: 25 cm^3/min	100 mtorr		300 W	> 26 nm/min	
CNT/Polyimide Composite (Initial)	ICP RIE	Silicon Nitride	O_2: 55 cm^3/min	50 mtorr	800 W	100 W	100 nm/min	20 nm/min
CNT/Polyimide Composite (Final)	ICP RIE	Silicon Nitride	O_2: 55 cm^3/min	50 mtorr	800 W	30 W	100 nm/min	5 nm/min
Cleaning Chamber	ICP RIE		O_2: 55 cm^3/min	50 mtorr	800 W	100 W		

Discussion

Patterning the composites requires their surfaces to be smooth. The AFM showed that

both of the composites had a RMS roughness lower than 61 nm over a 20 μm by 20μm area as a

result of hot pressing the composites against polished silicon wafers. The thickness of the

photoresist after being spin cast onto composites was about 2 μm, or about 35 times thicker than

the roughness of the composites and 1.33 times thicker than the largest step heights on supported

catalyst composites. This allowed us to effectively spin photoresist onto the composite sheets

and features on the micron scale. Even though supported catalyst composites could be patterned,

the step heights in the composites could be minimized or avoided by growing CNT forests with

more narrow rows.

Floating catalyst composites were difficult to etch due the iron oxide particulate

formation, micromasking the etched surface and lowering the oxygen plasma etch rate. Floating

catalyst composites can however be patterned by reducing the iron concentration by exposing the

44

composites to HCl where we believe the iron reacts with the HCl to form ferric chloride which is then rinsed off with water. Examining the iron concentration from the EDX measurements shows that the concentration began with about 10 wt% iron after the initial oxygen etch (fig 3.12a), decreased to 2.7 wt% iron after the HCl process (fig 3.12b), then increased to 15.2 wt% iron after an additional 40 min of etching (fig 3.12c). Iron concentration increasing after the final oxygen plasma etch suggests that more iron was exposed as the CNTs and polyimide were being etched. In order to continue etching through a thicker composite sheet, intermittently exposed to HCl vapor would be required between oxygen plasma etch steps to remove the iron buildup. Alternating between etching for 20 min and HCl exposure would allow etching through ~13 μm thick composite before a 400 nm thick silicon nitride would be etched through. This is assuming that the first 20 min of etching has an etch rate of 90 nm/min and that each additional 20 min of etching has an average etch rate of 150 nm/min. The oxygen etch process could be more efficient by adding a small amount of chlorine gas to the plasma. Chlorine gas would react with the iron in the composite to form ferric chloride gas (Ferric (III) chloride has a vapor pressure of approximately 55 mtorr at 187 °C[39]).

In contrast, supported catalyst CNT/polyimide composites did not show any signs of micromasking. As stated in the results section, EDX measurements on supported catalyst composites did not detect any iron. With an etch selectivity of 155:1 composite:silicon nitride, etching through a 62 μm thick composite would be possible before a 400 nm thick silicon nitride mask would be etched through.

When the composites were etched with the oxygen plasma, the etch rates tended to increase when the composites were not well attached to a silicon wafer. This suggests that the
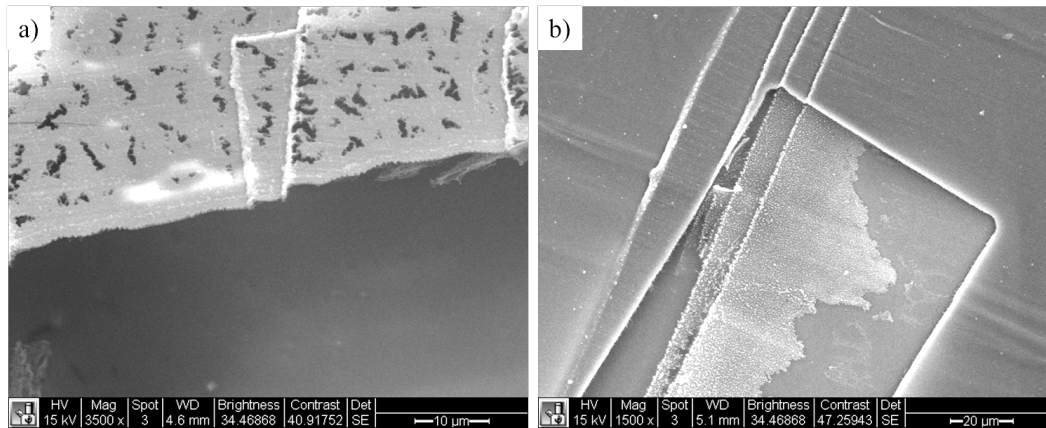
Figure 3.16 SEM images of supported catalyst composites after being oxygen plasma etched for 5 min. a) This composite detached from the wafer and was etched out from underneath the silicon nitride mask. b) This composite stayed well adhered to the wafer leaving the a-SiN mask and the covered composite intact.

thermal contact was insufficient and that the etch rates were temperature sensitive. The supported catalyst composites in figure 3.16 were etched at the same time for 5 min. The composite in figure 3.16a partially detached from the wafer and was etched out under the silicon nitride mask. The mask was also heavily damaged. When floating catalyst composites became detached from their carrier wafers, the composites did not etch out from under the silicon nitride masks, but the silicon nitride masks were severely compromised during the etch. This indicates that poor thermal transport causes the silicon nitride mask to heat up increasing the etch rate indicated by damaged areas on the mask (fig 3.16a). Some silicon nitride masks were damaged during etching even when the composites were still well attached to the wafer (fig 3.6b). To limit thermal problems while etching, the oxygen plasma etches were limited to 5 min with a 5 min pause repeated until the desired etch time was reached.

Conclusions

We have demonstrated a method to fabricate and pattern smooth, thin, high CNT density composite sheets. Hot pressing composites against polished silicon wafers proved to be an effective method in making the composites smooth enough for photolithographic patterning. Floating catalyst composites could only be etched effectively by reducing iron concentration, however during etching more iron was continually exposed causing a reduction in the etch rate. The iron micromasking in the floating catalyst composites, requires iron removal either during etching or in between etch steps. Supported catalyst composites were patterned through photolithography and etching. The faster etch rates and the lack of micromasking with the supported catalyst sheets allow them to be effectively etched with an oxygen plasma for use as microstructures.

BIBLIOGRAPHY

[1]   Peng, Bei, et al. "Measurements of near-ultimate strength for multiwalled carbon nanotubes and irradiation-induced crosslinking improvements." *Nature Nanotechnology* 3.10 (2008): 626-631.

[2]   Yu, Min-Feng, et al. "Tensile loading of ropes of single wall carbon nanotubes and their mechanical properties." *Physical Review Letters* 84.24 (2000): 5552.

[3]   McEuen, Paul L., Michael S. Fuhrer, and Hongkun Park. "Single-walled carbon nanotube electronics." *IEEE Transactions on Nanotechnology* 1.1 (2002): 78-85.

[4]   Pop, Eric, et al. "Thermal conductance of an individual single-wall carbon nanotube above room temperature." *Nano letters* 6.1 (2006): 96-100.

[5]   Bardes, Bruce P. *Properties and Selection: Irons and Steels*. 9th ed. Vol. 1. Metals Park, OH: American Society for Metals, 1978. 190,393. Print.

[6]   Weast, Robert C., Melvin J. Astle, and William H. Beyer. *CRC Handbook of Chemistry and Physics: A Ready-reference Book of Chemical and Physical Data*. Boca Raton, FL: CRC, 1985. Print.

[7]   Volder, M. F. L. De; S. H. Tawfick; R. H. Baughman; and A. J. Hart. "Carbon Nanotubes: Present and Future Commercial Applications." *Science* 339.6119 (2013): 535-539.

[8]   Lu, Shaoxin, and Balaji Panchapakesan. "Nanotube micro-optomechanical actuators." *Applied Physics Letters* 88.25 (2006): 253107-253107.

[9]   Hayamizu, Yuhei; Takeo Yamada; Kohei Mizuno; Robert C. Davis; Don N. Futaba; Motoo Yumura; and Kenji Hata. "Integrated Three-dimensional Microelectromechanical Devices from Processable Carbon Nanotube Wafers." *Nature Nanotechnology* 3.5 (2008): 289-294.

[10] Zhang, Guangyu, et al. "Selective etching of metallic carbon nanotubes by gas-phase reaction." *Science* 314.5801 (2006): 974-977.

[11] Cao, Qing, et al. "Medium-scale carbon nanotube thin-film integrated circuits on flexible plastic substrates." *Nature* 454.7203 (2008): 495-500.

[12] Zhou, Yangxin, et al. "P-channel, n-channel thin film transistors and pn diodes based on single wall carbon nanotube networks." *Nano Letters* 4.10 (2004): 2031-2035.

[13] Hutchison, David N., et al. "Carbon nanotubes as a framework for high-aspect-ratio MEMS fabrication." *Microelectromechanical Systems, Journal of* 19.1 (2010): 75-82.

[14] Barrett, Lawrence K., et al. "High-Aspect-Ratio Metal Microfabrication by Nickel Electroplating of Patterned Carbon Nanotube Forests." *Microelectromechanical Systems, Journal of* 24.5 (2015): 1331-1337.

[15] Coleman, Jonathan N.; Umar Khan; Werner J. Blau; and Yurii K. Gun'Ko. "Small but Strong: A Review of the Mechanical Properties of Carbon Nanotube–polymer Composites." *Carbon* 44.9 (2006): 1624-1652.

[16] Cheng, Qunfeng, et al. "Functionalized Carbon-Nanotube Sheet/Bismaleimide Nanocomposites: Mechanical and Electrical Performance Beyond Carbon-Fiber Composites." *Small* 6.6 (2010): 763-767.

[17] Wang, X.; Z. Z. Yong; Q. W. Li; P. D. Bradford; W. Liu; D. S. Tucker; W. Cai; H. Wang; F. G. Yuan; and Y. T. Zhu. "Ultrastrong, Stiff and Multifunctional Carbon Nanotube Composites." *Materials Research Letters* 1.1 (2013): 19-25.

[18] Liu, Ya-Nan, et al. "Ultrastrong carbon nanotube/bismaleimide composite film with super-aligned and tightly packing structure." *Composites Science and Technology* 117 (2015): 176-182.

[19] Cheng, Qunfeng; Jianwen Bao; Jingyu Park; Zhiyong Liang; Chuck Zhang; and Ben Wang. "High Mechanical Performance Composite Conductor: Multi-Walled Carbon Nanotube Sheet/Bismaleimide Nanocomposites." *Advanced Functional Materials* 19.20 (2009): 3219-3225.

[20] Liu, Wei, et al. "Producing superior composites by winding carbon nanotubes onto a mandrel under a poly (vinyl alcohol) spray." *Carbon* 49.14 (2011): 4786-4791.

[21] Bradford, Philip D., et al. "A novel approach to fabricate high volume fraction nanocomposites with long aligned carbon nanotubes." *Composites Science and Technology* 70.13 (2010): 1980-1985.

[22] Yoo, Kum-Pyo; Lee-Taek Lim; Nam-Ki Min; Myung Jin Lee; Chul Jin Lee; and Chan-Won Park. "Novel Resistive-type Humidity Sensor Based on Multiwall Carbon Nanotube/polyimide Composite Films." *Sensors and Actuators B: Chemical* 145.1 (2010): 120-125.

[23] Ozel, Taner, et al. "Polymer electrolyte gating of carbon nanotube network transistors." *Nano letters* 5.5 (2005): 905-911.

[24] Fang, Weileun, et al. "Polymer-Reinforced, Aligned Multiwalled Carbon Nanotube Composites for Microelectromechanical Systems Applications." *Advanced Materials* 17.24 (2005): 2987-2992.

[25] Ogasawara, Toshio; Yuichi Ishida; Takashi Ishikawa; and Rikio Yokota. "Characterization of Multi-walled Carbon Nanotube/phenylethynyl Terminated Polyimide Composites." *Composites Part A: Applied Science and Manufacturing* 35.1 (2004): 67-74.

[26] Cai, Hui; Fengyuan Yan; and Qunji Xue. "Investigation of Tribological Properties of Polyimide/carbon Nanotube Nanocomposites." *Materials Science and Engineering: A* 364.1-2 (2004): 94-100.

49

[27] Chou, Tsu-Wie; Limin Gao; Erik T. Thostenson; Zuoguang Zhang; and Joon-Hyung Byun. "An assessment of the science and technology of carbon nanotube-based fibers and composites." *Composites Science and Technology* 70.1 (2010): 119.

[28] Zhu, Bao-Ku, et al. "Preparation and properties of the polyimide/multi-walled carbon nanotubes (MWNTs) nanocomposites." *Composites Science and Technology* 66.3 (2006): 548-554.

[29] Zhou, Yuanxin, et al. "Experimental study on the thermal and mechanical properties of multi-walled carbon nanotube-reinforced epoxy." *Materials Science and Engineering: A* 452 (2007): 657-664.

[30] Lu, K. L., et al. "Mechanical damage of carbon nanotubes by ultrasound." *Carbon* 34.6 (1996): 814-816.

[31] Yi, Taechung, Lu Li, and Chang-Jin Kim. "Microscale material testing of single crystalline silicon: process effects on surface morphology and tensile strength." *Sensors and Actuators A: Physical* 83.1 (2000): 172-178.

[32] Petersen, Kurt E. "Silicon as a mechanical material." *Proceedings of the IEEE* 70.5 (1982): 420-457.

[33] Hopcroft, Matthew A., William D. Nix, and Thomas W. Kenny. "What is the Young's Modulus of Silicon?" *Microelectromechanical Systems, Journal of* 19.2 (2010): 229-238.

[34] Kovacs, Gregory TA, Nadim I. Maluf, and Kurt E. Petersen. "Bulk micromachining of silicon." *Proceedings of the IEEE* 86.8 (1998): 1536-1551.

[35] Wang, Ding, et al. "Highly oriented carbon nanotube papers made of aligned carbon nanotubes." *Nanotechnology* 19.7 (2008): 075609.

[36] Behnam, Ashkan, et al. "Nanolithographic patterning of transparent, conductive single-walled carbon nanotube films by inductively coupled plasma reactive ion etching." *Journal of Vacuum Science & Technology B* 25.2 (2007): 348-354.

[37] Wang, Teng; Di Jiang; Si Chen; Kjell Jeppson; Lilei Ye; and Johan Liu. "Formation of Three-dimensional Carbon Nanotube Structures by Controllable Vapor Densification." *Materials Letters* 78 (2012): 184-87.

[38] Tawfick, Sameh; Zhouzhou Zhao; Matthew Maschmann; Anna Brieland-Shoultz; Michael De Volder; Jeffery W. Baur; Wei Lu; and A. John Hart. "Mechanics of Capillary Forming of Aligned Carbon Nanotube Assemblies." *Langmuir* 29.17 (2013): 5190-5198.

[39] Rustad, Douglas S., and Norman W. Gregory. "Vapor pressure of iron (III) chloride." *Journal of Chemical and Engineering Data* 28.2 (1983): 151-155.

[40] Teo, Edwin HT, et al. "A carbon nanomattress: A new nanosystem with intrinsic, tunable, damping properties." *Advanced Materials* 19.19 (2007): 2941-2945.

[41] Gu, Aijuan, et al. "Bismaleimide/carbon nanotube hybrids for potential aerospace application: I. Static and dynamic mechanical properties." *Polymers for Advanced Technologies* 18.10 (2007): 835-840.

[42] Yun, Sungryul, and Jaehwan Kim. "Covalently bonded multi-walled carbon nanotubes-cellulose electro-active paper actuator." *Sensors and Actuators A: Physical* 154.1 (2009): 73-78.

[43] Vlassak, Joost Johan. *New Experimental Techniques and Analysis Methods for the Study of the Mechanical Properties of Materials in Small Volumes*. Diss. Stanford U, 1994. Ann Arbor: UIM.

[44] Liu, Chang. *Foundations of MEMS*. Upper Saddle River, NJ: Prentice Hall, 2012. Print.

[45] Ohring, Milton. *The Materials Science of Thin Films*. Boston: Academic, 1992. 182. Print.

[46] Spinks, Geoffrey M., et al. "Carbon-Nanotube-Reinforced Polyaniline Fibers for High-Strength Artificial Muscles." *Advanced Materials* 18.5 (2006): 637-640.

[47] Chandrashekar, A., et al. "Forming carbon nanotube composites by directly coating forests with inorganic materials using low pressure chemical vapor deposition." *Thin Solid Films* 517.2 (2008): 525-530.

[48] Ngo, Quoc, et al. "Thermal interface properties of Cu-filled vertically aligned carbon nanofiber arrays." *Nano Letters* 4.12 (2004): 2403-2407.

[49] Li, Jun, et al. "Electronic properties of multiwalled carbon nanotubes in an embedded vertical array." *Applied Physics Letters* 81.5 (2002): 910-912.